博士学位論文

μSR and DFT Investigations Quantum Electronic States of La_2CuO_4

（La_2CuO_4 中の量子的電子状態に関する μ SR と DFT による研究）

Muhammad Redo Ramadhan

北海道大学大学院理学院

物性物理学専攻

令和5年3月

μSR and DFT Investigations on Quantum Electronic Statse of La_2CuO_4

Muhammad Redo Ramadhan[1,2,3]

1. Department of Physics, Universitas Indonesia, Depok 16424, Indonesia

2. Department of Condensed Matter Physics, Hokkaido University, Sapporo 060-8010, Japan
3. Meson Science Laboratory, RIKEN Nishina Center, Saitama 351-0198, Japan

E-mail: muhammad.redo@ui.ac.id

Abstract

The muon spin relaxation (μSR) method is a powerful tool to investigate the electronic state of Cu-based high-T_C superconducting oxides. To reveal muon positions inside La_2CuO_4 gives us a useful information to achieve deeper understandings of the electronic states on its magnetically ordered state. However, any unified method to investigate muon positions have not yet been firmly established. For this reason, the μSR results achieved on La_2CuO_4 in the early stage of high-T_C history have not yet been fully explained. We are approaching this issue by using the density functional theory calculation method, with a supercell framework and including one muon as a dilute-charged impurity. The on-sites Coulomb potential, U, is included to achieve correct electronic states of the La_2CuO_4. By considering the quantum local effects caused by the implanted muon and the Cu-spin states in the La_2CuO_4, we finally succeeded to reveal the muon positions that corresponds well with the μSR experimental results. Adjusting the DFT and μSR results, we also optimized U to be 4.87(4) eV precisely, providing an accurate information of the electronic states in LCO and proposing a novel way to utilize μSR experiment on many strongly correlated systems.

Keywords: μSR, DFT, Muon Position, Distributed Spin, Zero-Point Energy

INTRODUCTION

Muon is one of the elementary particle, sharing its classification as the fundamental particle that have a half-integer spin (fermion) with the electron. Aside from the similarity on its spin, muon particles are always being thought as a heavier version of the electron. Hence, its unstable nature in the normal condition with the lifetime of 2.2 μs. It also has an antimatter version with an opposite sign of charge, resulting two kinds of muon particle (a positively charged and a negatively charged muons). Detailed comparisons with the other elementary particles are summarized in the Table 1 In this universe, muon can be produced naturally by an interaction of gases in the upper region of atmosphere with a sufficiently number of high-energy particles, which was observed by Carl D. Anderson and Seth Neddermeyer in 1936 [1]. Two decades later, Lee and Yang [2] proposed its theory that states that the parity conservation is exists in the strong interaction, but it does not exist within weak interaction regimme. This theory leads Garwin *et al.*, to implant the muon into the solids to test the theory [3]. Here they observed that the spin-polarized muon will retain its spin polarization when implanted into solid. This in acc-

Table 1. Comparison of elementary particles of electron, neutron, and muon

Properties	Electron	Muon	Neutron
Mass (m)	m_e	$207m_e$	$1840m_e$
Charge (q)	$\pm 1.6 \times 10^{-19}$ C	$\pm 1.6 \times 10^{-19}$ C	0
Spin (S)	½	½	½
Magnetic moment (μ_B)	$\pm 1.0011\mu_B$	$\pm 4.88 \times 10^{-3}\mu_B$	$1.71 \times 10^{-3}\mu_B$
Gyromagnetic ratio (γ)	28.02 $GHzT^{-1}$	135.4 $MHzT^{-1}$	183.3 $MHzT^{-1}$
Mean lifetime (τ)	4.6×10^{26} year	2.2×10^{-6} second	885 second

-ordance with the violation of parity conservation rule mentioned by Lee and Yang, that provide a unique and useful characteristic to probe the magnetic behavior in the systems. Currently there are four facilities which produce muon for condense matter studies. Paul Scherrer Institute (PSI) in Zurich, Switzerland and TRIUMF Laboratory in Vancouver, Canada. Both facilities utilized the continuous beam of muon. While RIKEN-Rutherford Appleton Laboratory (RAL) in Oxford shire UK and JPARC in Tokai, Japan provide the pulsed source of muon. Both source types of muon have their own advantages and disadvantages. In this thesis, there are six main sections: Introduction, Literature Review, Methodology, Results & Discussion, Reference, and Appendix. All μSR experiments are conducted by Budi Adiperdana and Dr. Isao Watanabe in PSI Switzerland. Several data in this thesis were reproduced with the permission Dr. Isao Watanabe and RIKEN which hold the rights of all experimental data conducted in PSI. Finally, in the appendix section, the author would like to include all published papers that author managed during the course.

LITERATURE REVIEW

In this section the author divide the literature review discussed within the thesis into four parts: basic knowledge of μSR spectroscopy, known exotic properties for the parent compound of La_2CuO_4 and related structure before finally the discussing on the theoretical approach to determine muon positions for several structures.

i) μSR spectroscopy

μSR is the abbreviation for muon spin relaxation, rotation or resonance depending on how the injected muons are expected to behave in the experiment. The μSR technique allow the user to inject the elementary particle of muon to act as a sensor for the electron spin dynamic in the microscopic scale. The injection of muon can be done by using either pulsed or continuous beam of muon. Due to its instability (muon's lifetime ~ 2.2 μs), the injected muon will decay into positron following the relation shown in Eq. 1. The positron then will be captured by the

$$
\begin{aligned}
p^s + p^t &\rightarrow \pi^+ + p + n \\
p^s + p^t &\rightarrow \pi^- + p + n \\
\pi^+ &\rightarrow \mu^+ + v_\mu \\
\pi^- &\rightarrow \mu^- + v_\mu
\end{aligned}
\tag{1}
$$

a detector which completes one (muon) data cycle. For one facility to produce muon, a proton beam with 600-800 MeV energy is required to be collided with the nuclei of target light element (graphite) [4]. As shown in Eq. 1, both negatively-charged and positively-charged muon are produced by using this procedure, however the negatively-charged muon tends to be attracted by the nuclei of the atom resulting a complex behavior between muon and the combination of nuclei and electron of the target material. In general, the positively-charged muon (μ^+) are the one that is mostly used in the condensed matter studies. In this thesis, all terms of muon(s) only refer to the positively-charged muon.

Important feature of the injected muon in the μSR studies is its weak parity violation nature that retain almost all of its spin polarization within muon's lifetime. By this logic, any possible changes to the muon spin polarization are caused by the spin dynamic of the target material. This way the injected muon will have an ability to reveal even a small and weak magnetic ordering originated from the target material. This feature is not apparent on other similar spectroscopy such as electron spin resonance (ESR) and nuclear magnetic resonance (NMR). Figure 1(a) shows a mechanism of μSR spectroscopy where the produced muons are guided to the target material, passing the muon detector before injected to the sample. Due to its spin, the injected muon will have a Larmor precession that corresponds to any possible magnetic

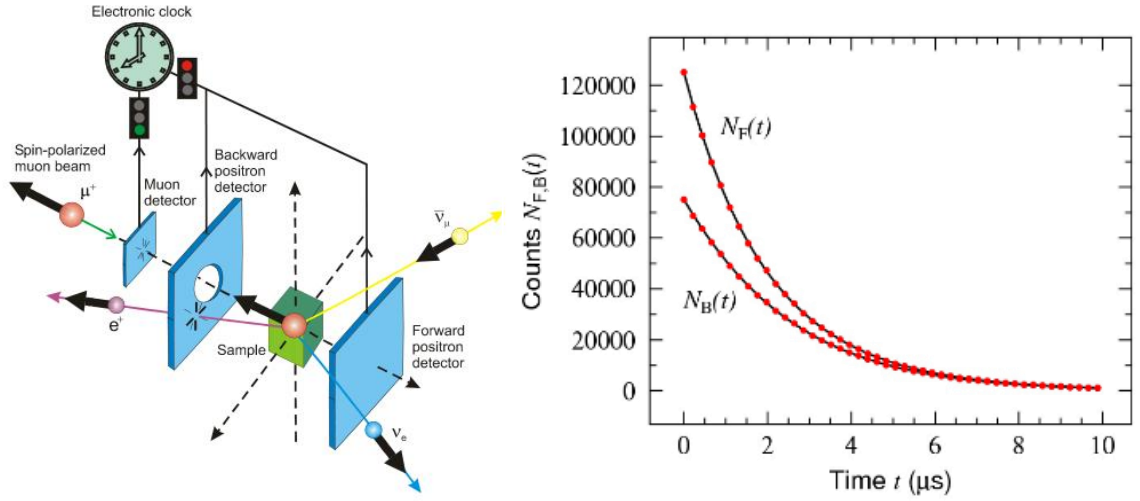

(a) (b)

Figure 1. (a) The Schematics of μSR spectroscopy. (b) The illustration of the total amount of detected positron by the forward and backward positron detectors.

ordering that target material possibly own. If the target material is known to have one simple magnetic ordering, then all of the injected muon will precess coherently or precess with a single frequency. This can only be happened if there is only one possible position for muon to be injected at within target material. In the case of complex material with several possible positions for muon, there will be also a number of precessing frequency that matched with the number of unique muon position in the material. In the process of muon spin precession, muon will decay into positron with its momentum aligned parallel to the spin precession of muon. All of positron will be captured and measured by the detector that is placed in the front and the back of target material. This process will be repeated in the period of time to obtain enough data (captured positron). The amount of captured positron is normalized into an asymmetry terms given by equation 2:

$$A(t) = \frac{N_B(t) - N_F(t)}{N_B(t) + N_F(t)} \quad (2)$$

The $A(t)$ term is the normalized data of positron i.e. possible asymmetry, N_F and N_B is the number of captured positron detected by the forward and backward detector respectively. From the equation 2, we can also obtained the information about its polarization, $P(t)$, by using the following equation:

$$A(t) = A_0 P(t) \quad (3)$$

with the A_0 term describes the initial asymmetry before the muon start to precess. All of the injected muons are known to precess with the frequency of $\omega_\mu = \gamma_\mu B_{int}$, in the case that the target material have a magnetic field with the value of B_{int}. The term of γ_μ is defined as the gyromagnetic ratio of muon with the value of 135.4 $MHzT^{-1}$ as written in Table 1. The magnetic field, B_{int}, is the total of seven different contributions and expressed as:

$$B_{int} = B_{con} + B_{trans} + B_{dip} + B_L + B_{dem} + B_{dia} + B_{ext} \quad (4)$$

The terms B_{con} and B_{trans} are the contributions from the hyperfine interaction between muon and all electrons in the vicinity of muon. Three terms of B_{dip}, B_L, and B_{dem} are originated from the dipole-dipole interactions within the sample material. The term B_{dia} is the diamagnetic field which commonly observed in the superconducting material. The term B_{ext} is a possible external field that is applied by the user to the target material to achieve a specific condition depending on the μSR experimental aim and goals. Note that not all of the terms will be considered and relied heavily on the target material's magnetic ordering. For instance, in the case of antiferromagnetic material, the term B_{dem} and B_L is not considered as these two related to the net magnetization of material. By using the equation 3 and 4, one is allowed to check the

possible changes of polarization over time that will produce a curve which can be fitted using specific polarization's functions and extracting the information of internal field value that is experienced by the injected muon within the target material.

ii) Known properties of La_2CuO_4 and related systems

La_2CuO_4 (LCO) is known as the parent compound of high-Tc superconducting system that is firstly observed in the late 1980. Interestingly, LCO has an antiferromagnetic insulating behavior which is against the basic idea on how magnetic and superconductivity relates to each other. It was understood that the magnetic impurities suppress the superconductivity for the case of conventional superconductors [5]. This means that the existence of magnetic ordering disrupts the superconducting behavior. In the case of doped-LCO, the antiferromagnetic and superconducting phase is really close and even coincides for the electron-doped sustem. Thus, one can pointed out that the important information about superconductivity of the cuprate system lies on its magnetic properties.

It was pointed out by Anderson after the discovery of high-TC superconductivity [6], that the LCO should be classified as Mott insulator with the super-exchange interaction which produces an antiferromagnetic correlation betwenn Cu and its neighbouring atoms. This opinion can be well understood within one-band Hubbard model [7]. For instance, within La_2CuO_4 system,there is one unpaired electron from the Cu^{2+} ions resides in the $d_{x^2-y^2}$ electronic orbital. Within the perspective of conventional band theory, the unpaired electron tends to delocalize

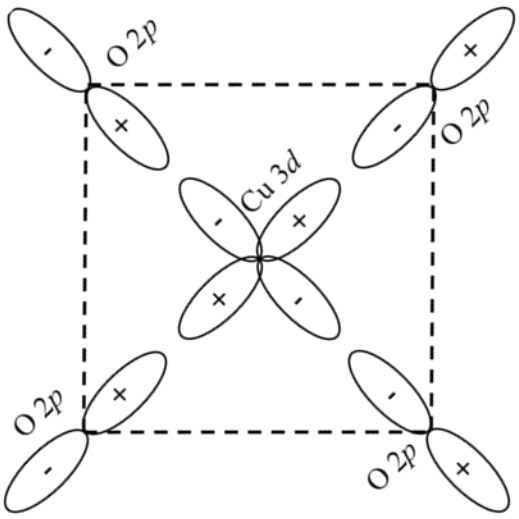

Figure 2. The schematic diagram of Zhang-Rice singlet formation, describing the hybridization of Cu $3d9$ hole and the doped $2p$ hole [8].

itself to reduce the energy by moving to the neighbouring Cu-site suggesting that the system should behave as a normal metal. However, the experimental study on the LCO describes that

the LCO system behave as an insulator with 2 eV electronic band gap [9]. In this scenario, one possibility that forces the LCO to behave as an insulator is the effect of large on-site Coulomb repulsion (U) that is required to be larger than the width of the d-orbitals between two Cu which localize the unpaired electron and shows an insulating characteristics. It is still possible for the unpaired electron to delocalize itself, by moving to the nearest Cu-sites on the condition that the neighbouring Cu atom should have an antiparallel spin which then realizes both antiferromagnetic and insulating characteristics. The Hamiltonian for Hubbard parameter in the LCO can be described by:

$$H = -t \sum_{i,j,\sigma} c_{i\sigma}^{*} c_{j\sigma} + U \sum_{i} n_{i\uparrow} n_{i\downarrow} \tag{5}$$

here, the term i is the index for the central atomic site, while the term j is the index of neighbouring atomic site. The term σ is the index for the electron spin. In equation 5, the first term explains the electronic exchange that arises due to the atom in the central and neighbor sites respectively. While the second term shows the required energy for two electrons to be in the same atomic site of i. The term t is known as a transfer integral for two electronic states that overlap with each other within the tight-binding model. For the superconducting case, the one-band Hubbard model is not enough to explain the superconducting phenomena as it was shown that the holes that originated from the Sr/Ba atoms doping process tend to localize in the O 2*p*-orbital. Hence, the three-band Hubbard model is designed specifically involving Cu $3d_{x^2-y^2}$ and Op_x,Op_y orbitals in order to explain superconducting phenomena. Later on, Anderson states that one-band Hubbard model is sufficient to describe many important feature within the superconducting cuprate, but still unclear on why one can ignore the contribution of oxygen atom in describing superconducting feature [6]. Finally, the confusion is addresed by Zhang and Rice [8], where they showed that a singlet orbital structure between Cu $3d_{x^2-y^2}$ and O 2*p*-orbitals in the CuO_2 plane has a lower energy compared to the orbital structure of non-bonding triplet. This suggests that the hole from the parent compound and the doping atom are scattered around the Cu and O sites within a single-orbital structure near the Fermi surface, allowing the energy penalty from the one-band Hubbard model to be ignored. In such case, the previous Hamiltonianian can be reconstructed into:

$$H = -t \sum_{i,j,\sigma} c_{i\sigma}^{*} c_{j\sigma} + J \sum_{i,j} S_i . S_j - \frac{1}{4} \tag{6}$$

here the terms t and J are the transfer integral parameter and the exchange coupling respectively. This model is known as the $t-J$ model and proven to be sufficient in the

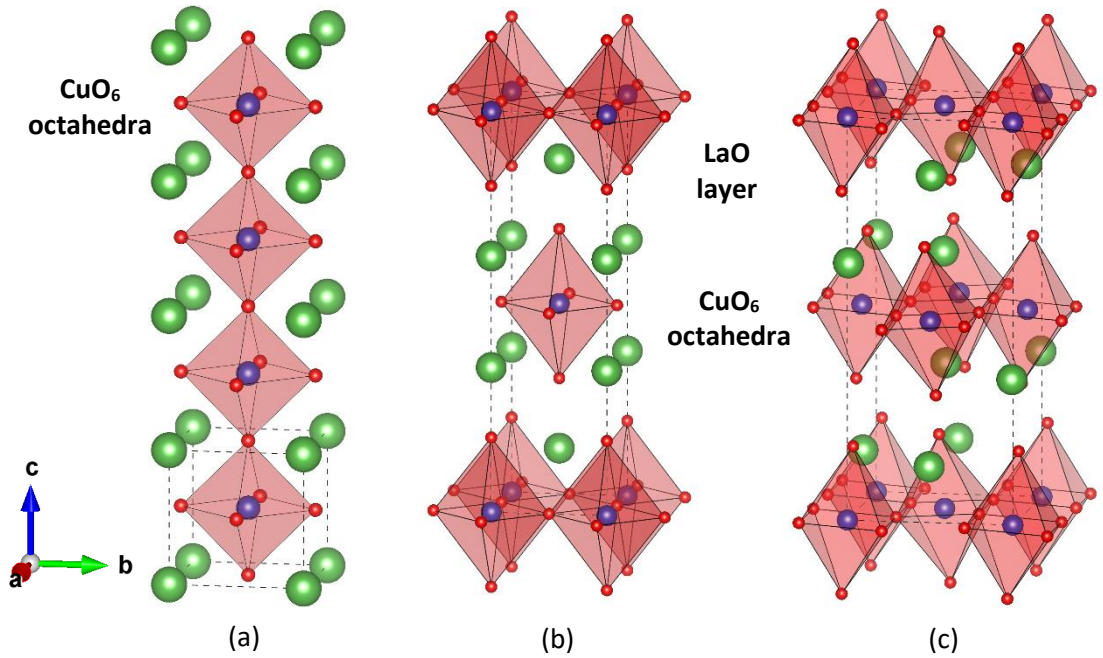

Figure 3. Crystal structure description of (a) Perovskite ABO_3 (b) High temperature tetragonal La_2CuO_4 (c) Low temperature orthorhombic La_2CuO_4. Dashed line indicates the unit-cell for each system

temperature variation of 100 K – 1000 K. In the hole-doped variation, the singlet formation on the CuO2 plane has a non-magnetic behavior due to half integer spin owned by both original and doped holes. Looking at the cuprate phase diagram, the antiferromagnetic ordering is vanished suddenly even for a small amount of hole-doping content (at 0.02). In contrast, the magnetic Cu-atom need to be substituted partially with the non-magnetic atom using the compositio of 60:40 to destroys the antiferromagnetic ordering in the system. Here, we can deduce that the aforementioned singlet orbital structure is correlated strongly with the antiferromagnetic behavior of the LCO system, either by decreasing the magnetic moment of Cu or by destroying the magnetic order by the "movement" of the hole. From the μSR data on LSCO and YBCO system, the second transition of magnetic state was observed at 25 K for the small percentage of doping content at 1% to 3% [10]. This magnetic behavior in the doped system suggest a possible existence of localized spin from the doped holes. Increasing the doping content causes the system to undergoes another transition to the spin-glass state that coincides with the superconductivity. All of the characteristics mentioned above is detected on both LSCO and YBCO system, showing that the exchange interaction on both system is similar. From those data we can argue that there is some correlation between superconductivity and magnetism for the hole-doped case. The magnetic characteristic on its parent compound is not killed immediately by small amount of hole concentration and possibly correlated with the

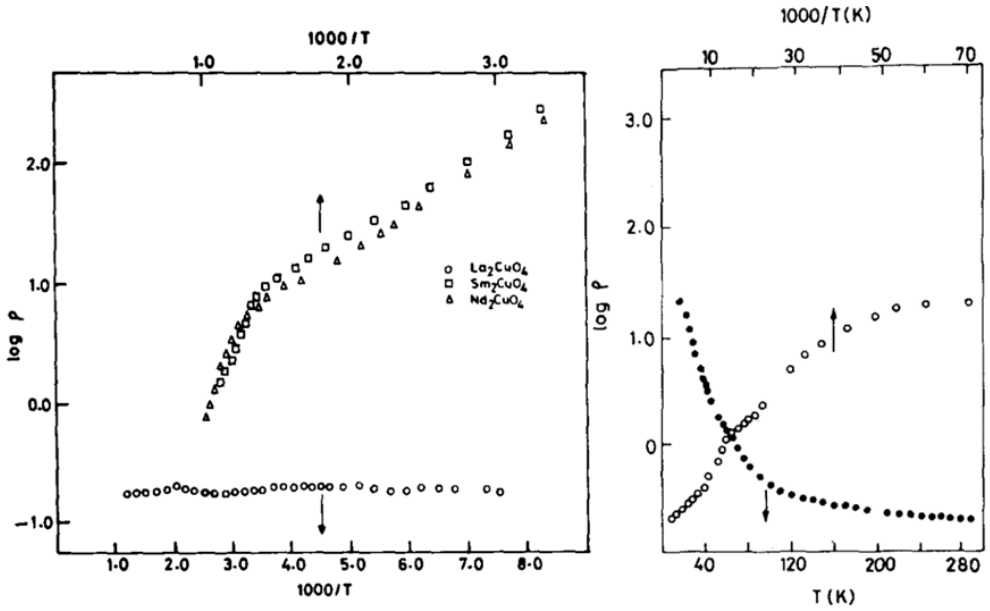

Figure 4. Electrical resistivity vs temperature data (a) Ln_2CuO_4 (Ln = La, Sm, Nd), for temperature range of: 1000 K-125 K [17] (b) La_2CuO_4, for temperature range of: 280 K-14 K [18].

existence of superconductivity on further doping. Therefore, discussing on the magnetic behavior on the parent compound deeper is one way to have a better understanding on the sup--erconducting behavior in cuprate system.

La_2CuO_4 crystal structure can be considered as a derivation from the related structure of perovskite type with the stoichiometric composition of ABO_3. This class of material is known for its variation of physical and electronic properties such as: the ferroelectricity ($BaTiO_3$), the ferromagnetism ($YTiO_3$), the ferroelasticity ($SrTiO_3$), and the pyroelectricity ($LiTaO_3$) [11-15]. For this class of materials the term of A and B are defined as two different-sized cations, which then combined with the oxygen (O) ions. The B ion (smaller cation) form a BO_6 octahedral structure with the A ion as the foundation on the corner of the ABO_3 lattice which forms a cubic structure. Other properties of perovskite-type structure is its stability on different atomic composition, forming additional derived structure easily. In case of La_2CuO_4, the CuO_6 octahedron is combined with LaO layer forming K_2NiF_4 crystal structure. In the high-temperature regimme of 535 K, the La2CuO4 stabilizes in the tetragonal crystal structure that is defined as high temperature tetragonal (HTT) with the l4/mmm space group. Near the room temperature, La_2CuO_4 transforms into orthorhombic crystal structure that is defined as low-temperature orthorhombic (LTO) with the space group of Bmab [16]. The latter transformation is followed by the changes on the atomic bond distance for each atom as the temperature is lowered. In order to lower its energy, each CuO_6 octahedra is tilting to one side followed by the neighbouring octahedral tilting to the other side. In the LaO layer, the La atom is also moved

to the b-direction as shown in figure 3. For the La_2CuO_4 and similar structure such as La_2NiO_4 there is no sign of second transition to the low-temperature tetragonal structure and retain its original low-temperature orthorhombic structure [19].

Early experimental studies on the Ln_2CuO_4 structure where Ln is the three of Lanthanides group (La, Sm, and Nd) shows that both Sm_2CuO_4 and Nd_2CuO_4 behaves as an insulator from high temperature to the low temperature, La_2CuO_4 is classified to be metal at that time due to its much smaller value of resistivity [17]. Further data shows that, the resistivity curve is close to be constant when the variation of temperature at 1000 K – 125 K is introduced as shown in figure 4(a). Later study shows that the resistivity value is increasing sharply below 100 K temperature mark suggesting that for the low temperature region La_2CuO_4 behaves as an insulating system[20]. However, the increase of resistivity value is strongly depends to the stoichiometric composition of the compound, making it unclear whether the sharp increase is an intrinsic feature or not. Uchida et al., support this finding and shows a 10^4 order difference between resistivity of stoichiometric La_2CuO_4 when measured at 10-100 K [18], suggesting that the insulating characteristic of La_2CuO_4 is an intrinsic feature of the system. Neutron diffraction experiments on the powdered sample of La2CuO4 system shows that an existence of antiferromagnetic transition at the lower temperature region. This transition follows the similar characteristic of the resistivity measurement, where the transition temperature is also strongly dependent on the stoichiometric of the sample. Vaknin et al., shows a strong magnetic peak at the (100) scan at the measured temperature of 220(10) K, which shows that the antiferromagnetic ordering is aligned to the y-direction [21].

iii)Injected muon positions of La_2CuO_4 based on theoretical studies

As described in the first sub-section of literature review, the μSR spectroscopy have a strong sensing capabilities on a weak internal field. However, it is still unclear on how to determine the exact stopping position of the injected muon within the target material. Couple methods had been proposed to remedy this problem. In the specific case of La_2CuO_4 and its relative LSCO, there were two common methods that is used to determine the position of injected muon. First is the dipole field method, and second is the first principle methods. The first method is based on Hitti et al., study. They utilize the magnetic dipole method to obtain a possible position of injected muon by comparing the magnetic dipole field value with their own experimental μSR data. The following equation is required to obtain the position:

$$H_i = \sum_i \frac{\mu_i}{r_i^3}[3(\mu_i \,.\, r_i)r_i - \mu_i] \qquad (7)$$

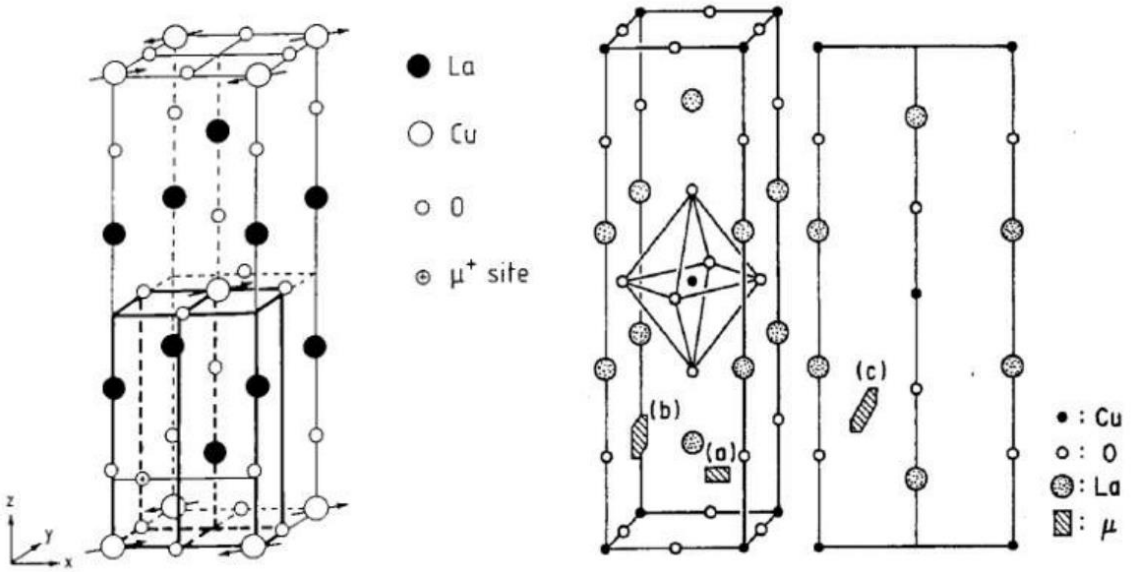

Figure 5. Proposed injected muon positions based on electronic and nuclear dipole field method.

Here the i term defines the index for the Cu magnetic atom that has a magnetic moment, μ_i, surrounding the injected muon. The term of r describes the distance of muon to all of the surrounding Cu magnetic atom. Following this method, Hitti et al., utilized an antiferromagnetic structure with the magnetic moment of 0.48 μ_B/Cu-atom as observed by the neutron diffraction study [21]. By using this magnetic moment value and their internal field value (428 G) extracted from the μSR data, Hitti et al., observed seven possible position for the injected muon position after limiting the possible position with the assumption that muon only stop at the ac-plane on the crystal structure. Table 2 summarize all possible position [22].

Table 2. Injected Muon Coordinate with its respective calculated internal field

Position	x/a	x/b	x/c	Description	H_{int} (mT)
1	0	0	0.5	Interstitial CuO2 planes	135
2	0	0	0.25	Interstitial ¼ C	0.5
3	0	0	0.184	Vacancy, O-chains	28.1
4	0.5	0	0	Vacancy, O-planes	0
5	0.5	0	0.184	Interstitial, O-O bond	29.4
6	0.5	0	0.25	Interstitial, middle face	19.4
7	0.253	0	0.253	Interstitial $d(\mathrm{O}-\mu_i)-1$ Å	42.8

In this table, it was shown that the most possible position based its internal field and distance to the nearest oxygen is position 7. While position 5 has the closest value to the experimental

results, the distance of this coordinate to the closest oxygen position is 1.9 Å. As the theoretical approximation of muon and oxygen atom should be around 1 Å (based on the assumption that muon ~ hydrogen), the position 5 is not considered as the real position. Hitti et al also mentioned that the injected muon tends to bond with the apical oxygen as observed in this study. Other study based on the dipole field method is also done by Torikai et al., [ ]. Here they used the nuclear dipole field instead of the electronic dipole field which follows this equation:

$$M_{2,single}^{ZF} = \begin{cases} \left(\hbar\gamma_\mu\gamma_N\right)^2 \sum_i \frac{1}{3} I_i(I_i+1)(2+3\sin^2\Omega_i)\frac{1}{r_i^6} \\ \left(\hbar\gamma_\mu\gamma_N\right)^2 \sum_i \frac{1}{3} I_i(I_i+1)\,4\sin^2\Omega_i\frac{1}{r_i^6} \\ \frac{1}{3}\left(\hbar\gamma_\mu\gamma_N\right)^2 \sum_i I_i(I_i+1)\left[4\sin^2\Omega_i + \frac{3}{4}\frac{I_i+\frac{1}{2}}{I_i(I_i+1)}(2-\sin^2\Omega_i)\right]\frac{1}{r_i^6} \end{cases} \quad (8)$$

The I_i term is defined as the spin for the nuclei, the term of Ωi is determined to be the angle between spin polarization of injected muon and r_i that describes the distance between muon to every atom that is considered in the calculation. It is known that La2CuO4 system have $I_{Cu} = 3/2$ and $I_{La} = 7/2$, these two defintion is known as possible nuclear spin distributions. Based on the calculation distance of 25 A, and comparing the second moment value from the μSR experimental data, three regions are considered to be most plausible location as shown in Figure 5. Region a and Region b are positioned at the (100) and (010) planes. It is also observed that the distance of this regions with the apical oxygen is close to 1 A. Region c is located between two apical oxygen at the (110) plane with the averaged calculated distance of 1.6 A for both nearest apical oxygen. Next is the first-principle method which considers the injected muon positions based on the total energy of the system. Here, the injected muon is taken to be a positive charge which goes into the electronic system. McMullen et al., shows that for the $YBa_2Cu_3O_7$ and $Bi_2Sr_2CaCu_2O_8$ systems the most possible coordinate for muon is the top of apical oxygen with the muon-oxygen distance is calculated to be 1.27 Å [23]. Sulaiman et al., shows that based on the unrestricted Hartree-Fock (UHF) approximation, the modelled muon atom (hydrogen) that is placed in the chosen atomic clusters. Here they restrict the coordinate to be the one that have a distance of 1 Å to the nearest oxygen. By varying its angle then calculate its energy for each angle, they conclude that the most possible position is angled at 25^o of apical oxygen position. Interestingly they also mention second possible position which is located at the planar oxygen with an angle of 55^o. From three studies mentioned before, the exact position is still cannot be said as there are several limitation they used to limits the

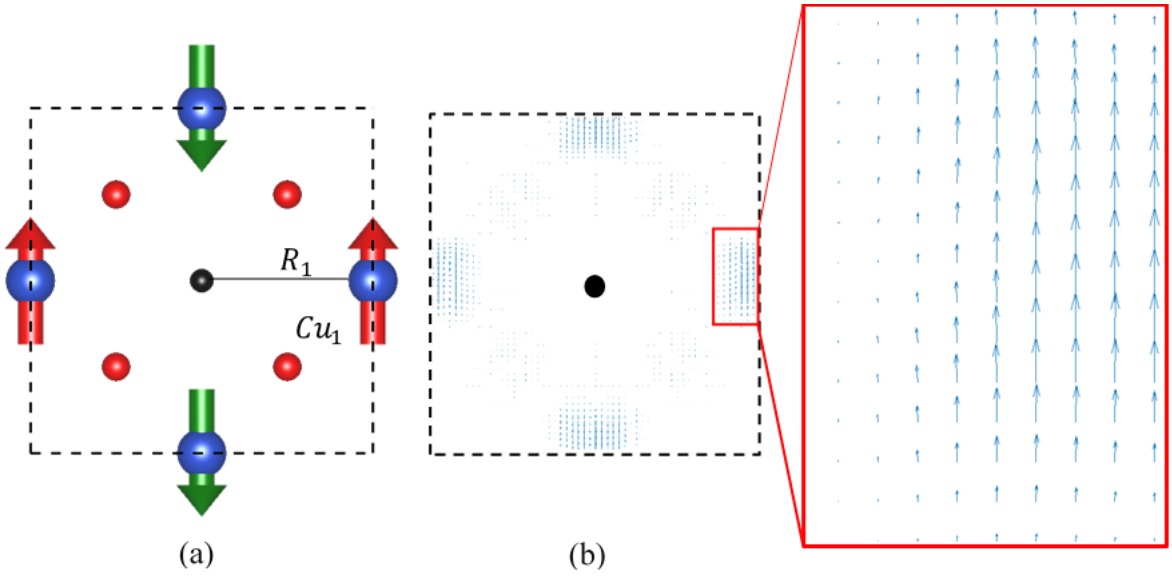

Figure 6. Visualization of (a) Point-Spin Approximation (b) Distributed-Spin Approximation

calculation. Furthermore, exact comparison with the experimental data is also missing, thus the unified method to obtain accurate position of muon is arguably still missing.

Methodology

Density functional theory (DFT) is an approximation method to determine the ground state energy of an interacting system with a large number of electrons. DFT calculation is performed using the projector augmented-waves (PAW) formalism as implemented in the Vienna *Ab-initio* Simulation Package (VASP) code [25,26]. The exchange-correlation functional GGA-PW91 was utilized by adjusting U between 2-8 eV to realize the insulating behavior of La2CuO4 structure [27]. The antiferromagnetic spin configuration of LCO is constructed based on the spin structure that was estimated from the neutron diffraction studies and aligned to the *b*-axis. The structure that was used throughout this study is determined to be the orthorhombic with the *Bmab* space group and lattice parameter value: a = 5.3568 Å; b = 5.4058 Å; c =13.1432 Å. Two kinds of structure were considered on this summary, that is the unit-cell structure and the 32-units supercell structure of La2CuO4 in the arrangement of 4 × 4 × 2. Brillouin zone sampling is done in 6 × 6 × 3 k-points for the unit-cell structure and a single gamma k-points for the 32-units supercell structure. The calculation on this study is divided into two stages. The first stage is focused on how we can obtain correct electronic structure. Second stage of calculation will be focused on how the muon affects the local structure that is aimed simulates the experimental condition in μSR spectroscopy. Internal field that was felt by muon comes mainly from the dipole interaction between the muon and the surrounding spins of Cu, and can be written as:

$$B_{dip} = \frac{\mu_0}{4\pi} \sum_i \frac{3(\mu_i^{Cu}.\hat{r})\hat{r} - \mu_i^{Cu}}{|R_i|^3} \quad (9)$$

The term of μ_0 is defined as the vacuum permeability,the $\hat{r}$ is the unit vector, and R_i is the distance between the center of position, and magnetic moment of Cu atom (μ_i^{Cu}). In this thesis we consider both point-spin model and the distributed-spin model. While it is known that the spin should be distributed, this model is not so often considered. This is due to the effect should be minimal for the situation of two different spins (atom). As the injected muon is considered to be located at the interstitial sites, it should have larger effects for the distributed-spin considerations. The distributed-spin structure of La_2CuO_4 is taken from the DFT calculation using the non-collinear calculation so the distributed-spin have 3 component of $x, y,$ and z. The final consideration that will be included for the internal field calculation is the zero-point vibration motion of the muon. As a fine particle, muon should behave like a quantum particle does, where in the lowest energy (ground state), muon will actually fluctuate around its minimum instead of constantly stop at single energy. The eigenstates for the muon's particle can be evaluated by:

$$\left[\frac{\hbar^2}{2m_\mu}\nabla_i^2 + V_\mu^{Hartree}(r)\right]\Psi_\mu(r) = E_\mu\Psi_\mu(r) \quad (10)$$

where m_μ refers to the mass of muon, and the $|\Psi_\mu|^2(r)$ is the probability for muon to beresides on each position r. The Schrödinger equation will be solved by utilizing numerical methods of finite different. This calculation will give us probability density map which will be considered for our internal field calculation.

Results & Discussion

The high-intensity μSR experiment was done in the Paul-Scherrer Institute (PSI) Switzerland by using continuous muon beam. The target for this study is a large single crystal of La_2CuO_4 with Neel temperature determined to be 325 K from SQUID experiment. The sample is also confirmed to be a single phase with no impurity by using X-Ray diffraction measurement at room temperature. Figure 5(a) is the zero field μSR (ZF-μSR) time spectra of La_2CuO_4 measured at temperature of 1.7 K, within the time window of 3 μs. Clear muon-spin precession is observed on this figure, indicating the behavior of the long-range antiferromagnetically ordered on La_2CuO_4 system. By performing fast Fourier transform (FFT) on the spectra and filtered the time spectrum we obtain the open circle curve as shown on the

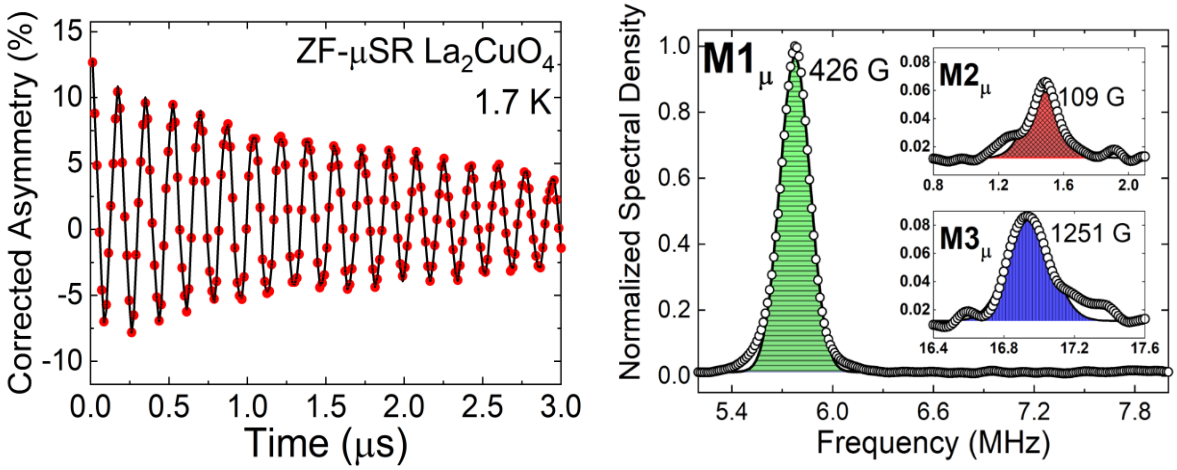

Figure 7. μSR time spectrum with its respective Fourier transform peak measured at 1.7 K on the La_2CuO_4 single crystal

Figure 5(b). Furthermore, we fit those curves using the Gaussian function that is described by the solid black lines. We determined that the highest peak is observed at the frequency around ~5.78 MHz which also observed on any past μSR studies on LCO. Two additional fields were observed and determined to have ~1.48 MHz and ~17.0 MHz frequencies. We named 3 unique frequencies as $M1_\mu$, $M2_\mu$, and $M3_\mu$. It was known that the highest intensities ($M1_\mu$) always observed on past μSR studies, while $M2_\mu$ is observed on thin film and single crystal [28-30]. Third frequencies of $M3_\mu$ is the newly found and can be originated from the combination of our high-quality sample and high-intensity of the experiment. Using the gyromagnetic ratio of muon $\gamma_\mu = 135.5$ MHz/T and the relation between muon-spin frequencies and internal field (B_{int}) of $\omega_\mu = 2\pi\gamma_\mu B_{int}$, we determined the internal field values are 426.7(1) G, 109.2(4) G, and 1251.6(3) G for for $M1_\mu$, $M2_\mu$, and $M3_\mu$ respectively.

To reveal the connection between the μSR experimental data and DFT calculation, we first performed the DFT calculation with the inclusion of Hubbard, U. Figure 6 describes the band structure of unit-cell LCO for the case of $U = 0$ eV and $U = 5$ eV. The significant changes that we can observe is the missing of the electronic gap at the Fermi level making the calculated ground state for $U = 0$ eV is a metal. The antiferromagnetic configuration is still retained, albeit with a nearly nonexistent total magnetic moment value at ± 0.002 μ_B/Cu-atom. This result highlights the importance of the inclusion of U-values to achieve a comparable result with the experiment. For comparison the magnetic moment of La_2CuO_4 at $U = 5$ eV is calculated to be ± 0.52 μ_B/Cu-atom. Another difference can be observed by drawing partial bands of Cu $d_{x^2-y^2}$ orbital (colored bands on the figure), where the splitting of upper Hubbard

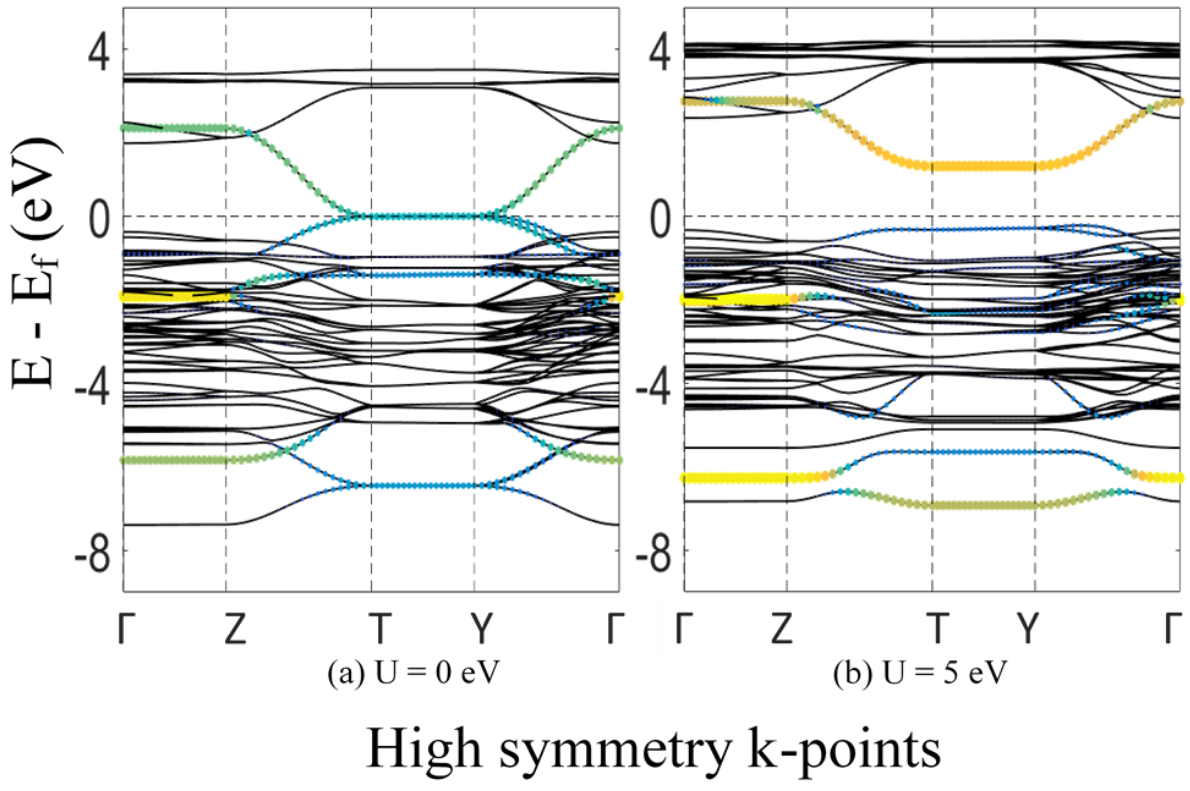

Figure 8. The bandstructure of La_2CuO_4 with different applied U-value for Cu 3d-orbitals. Colored lines describes the Cu $3d_{x^2-y^2}$ band

band (UHB) realizing the half-filled states which is very common for the Mott insulator systems. Similar splitting can also be seen in the lower Hubbard band (LHB).

To determine the possible position of the muon inside the system, we calculate the electrostatic potential of the muon within DFT formalism. Figure 7 shows the possible muon positions determined by measuring the unique minimum/maximum value inside the electrostatic potential. We observed that there are at least three unique minimum/maximum values located near the CuO_4 octahedron. In this figure, the colored slice section covers 1.06 eV potential energy from the most minimum value. Three unique muon positions are labelled as $M1_{DFT}$, $M2_{DFT}$, and $M3_{DFT}$ respectively, based on its potential value. $M1_{DFT}$ is determined as the most minimum (in respect to the muon positive charge) with the potential value of -11.31 eV, followed by $M2_{DFT}$ at -11.16 eV and finally -10.33 eV for the $M3_{DFT}$ position. $M1_{DFT}$ and $M2_{DFT}$ positions are located in the vicinity of the apical oxygen, while $M3_{DFT}$ is located on close proximity with the CuO_2 plane. Now we discuss about the possibilities of several states of the muon captured in the experiment. As discussed in the first section on this chapter, there are only two reports which produce the several states of the muon in both thin film and single crystal samples. Both showing additional lower internal field at around ~100 G

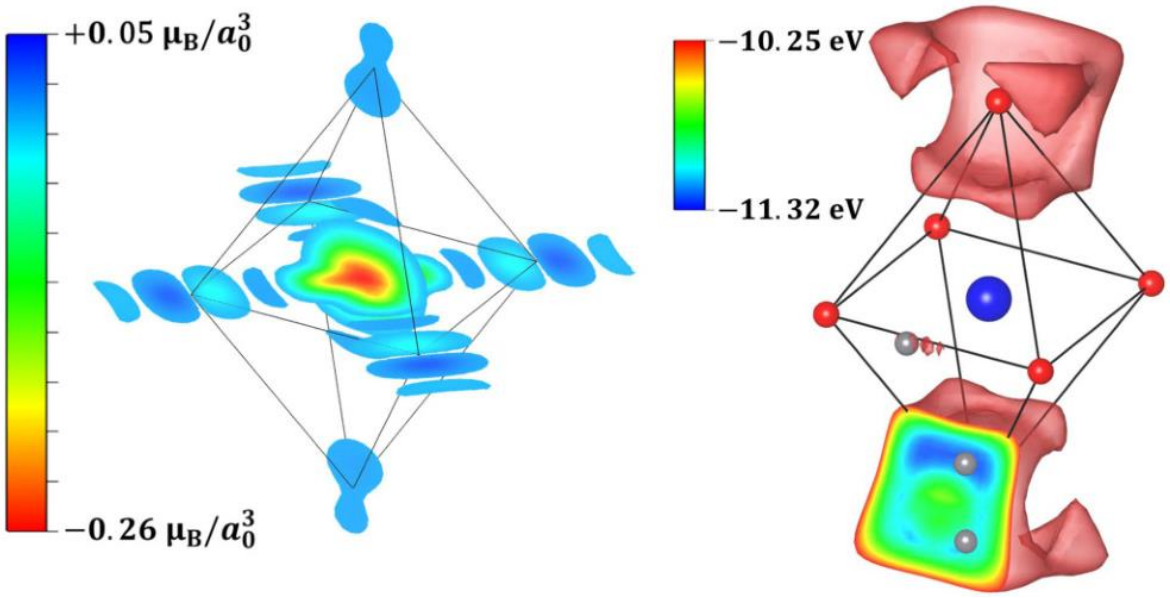

Figure 9. Three-dimensional representation of spin density and electrostatic potentnial.

with the major internal field at around ~400 G and no evidence of the existence of third internal field that was detected on this study. These facts are very similar to what was observed from our calculation, where two lowest minimum value (highest possibilities for muon to be resides in) and the states of the third lowest minimum follow the logic of our μSR experiment. If we consider that the most minimum, $M1_{DFT}$ position as the possible source for the $M1_{\mu}$ internal field. Then the $M2_{DFT}$ which has larger distance to the Cu atom compared to the $M1_{DFT}$ should have a smaller internal field. For the $M3_{DFT}$ position, large potential barrier from the $M3_{DFT}$ makes it difficult for the implanted muon to be resides in this position statistically. In this case, the high-statistics, μSR experiment is required in order to reveal the third internal field. Furthermore, the position of the $M3_{DFT}$ is very close to the Cu atom which effectively increases the internal field that is experienced by the muon on this position, consistent with our finding on the highest internal field for $M3_{\mu SR}$.

We also introduce the structural deformation caused by muon for our studies by using the supercell structure of La_2CuO_4 and including single hydrogen atom at the possible muon position as discussed in previous paragraph. Figure 8 shows the local deformation caused by muon estimated from DFT to the local structure of CuO_4 octahedron. We also confirm that the effect is mostly local, where only next nearest neighbor of octahedron that is affected and vanish completely near the boundary of supercell structure. $M1_{DFT}$ that is initially located near the apical and just outside of the CuO_4 octahedron, goes inside the octahedron the structural optimization. This movement of $M1_{DFT}$ causes the nearest Cu atom to be pushed upward 0.22 Å from its original position. The optimization of $M1_{DFT}$ also causes the planar Oxygens to be

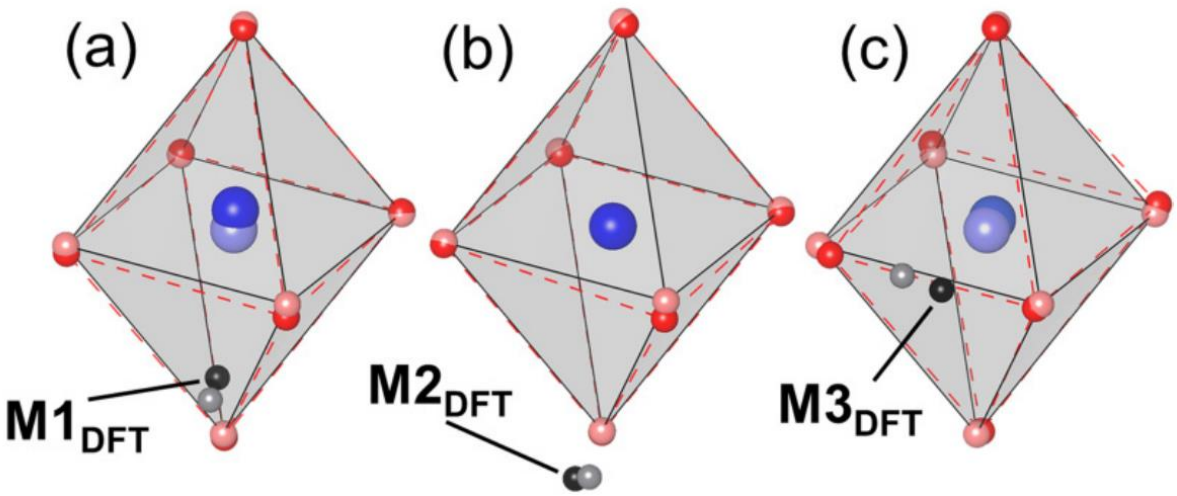

Figure 10. Effect of injected muon for to the local structure of CuO_6 octahedron

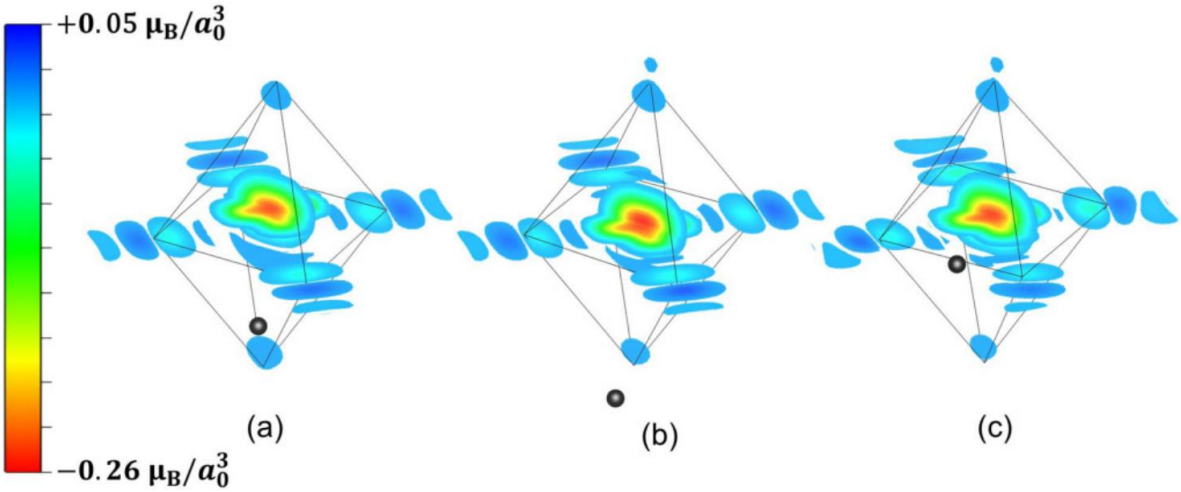

Figure 11. Spin density distribution calculated for La_2CuO_4 with applied $U = 5\ eV$ with the injected muon is placed at the most minimum position based on the electrostatic potential.

pulled on the direction of the $M1_{DFT}$. For the $M2_{DFT}$ position, muon also resides near the apical Oxygen and goes away slightly and pulled the same planar Oxygen slightly just like the $M1_{DFT}$ cases. No movement for the Cu atom in this case, due to the large distance between the $M2_{DFT}$ with the Cu atom. For the $M3_{DFT}$, muon stays just in between two planar Oxygens and with the structural optimization, muon pushes away the Cu atom from its original position and pulls the surrounding planar Oxygens into muon position after the optimization. Similar behavior also observed on the spin structure, where the nearest Cu-spin is slightly affected whereas the near-boundary Cu-spin is still retained. The final consideration that we included on this study is the zero-point vibrational energy. As discussed previously, the zero-point vibrational energy obtained can provides the probability density map to realize the muon as a fine quantum particle. Figure 9. describes the probability density of muon within the $1.5 \times 1.5 \times 1.5$ Å cubic box. We can observe that the injected muon's probability to resides in is stretched out

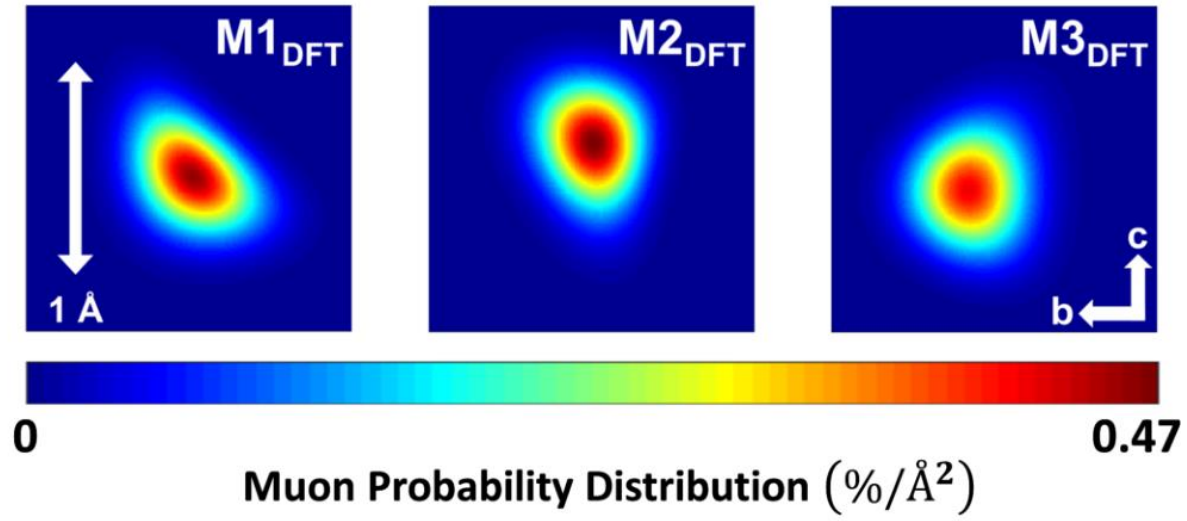

Figure 12. Zero-point vibration motion of the muon around the electrostatic potential anisotropically around the optimized muon position. The shape of this probability density is strongly related to the potential shape of the muon.

The final step is to obtain all of the mentioned parameter using the variation of U-values and calculate the internal field using the following equation:

$$H_{int} = \sum_{i,j} \frac{1}{|\vec{r}_i - \vec{r}_j|^3} \left[3\vec{\rho}_i . (\vec{r}_i - \vec{r}_j) \frac{(\vec{r}_i - \vec{r}_j)}{|\vec{r}_i - \vec{r}_j|^2} - \vec{\rho}_i \right] |\varphi_j|^2 \qquad (11)$$

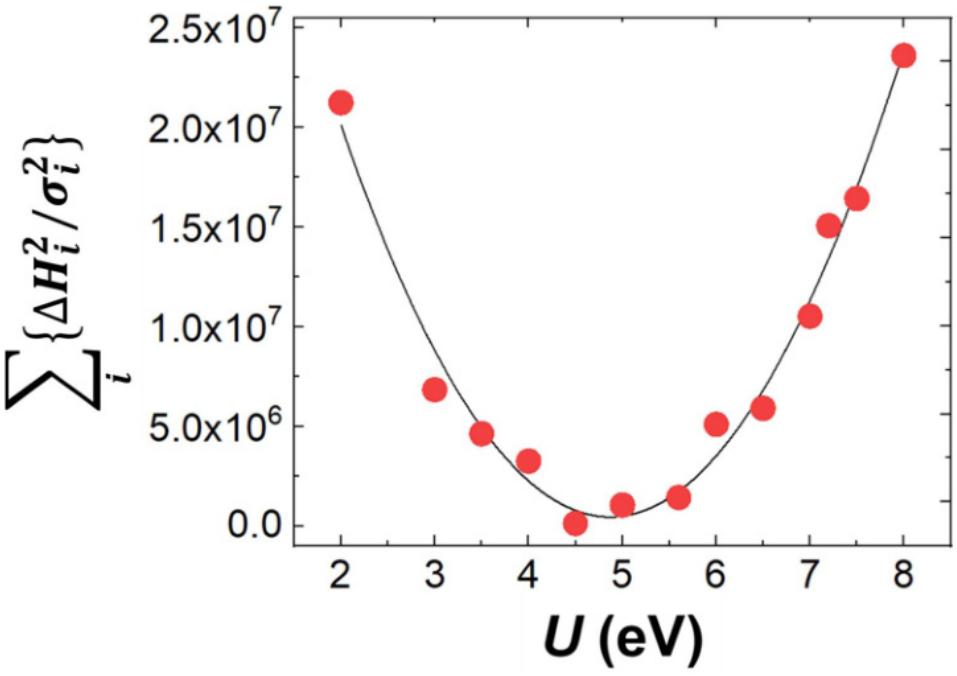

Figure 11. Optimization of U-value in respect to the internal field obtained by both μSR experiment and DFT calculations. Black solid line shows the best-fit results utilizing Gaussian function

with the $|\varphi_j|^2$ describes the probability density of muon. Then we summed up all grid components from our spin-density and the probability density to calculate the internal field at the designated muon position. Table 3. summarizes all of the DFT parameters obtained within this study. Compared to the point-spin model with the distributed-spin and deformation effects, further reduction is observed, increasing its accuracy compared with the μSR experimental results. In Table 3 we can easily estimate that the best *U*-values for La_2CuO_4 are within 4-7 eV, confirming the known experimental techniques to for the *U*-values estimation [31,32]. Furthermore, we can take a step further to the determine the best *U*-values by considering the asymmetry ratio of the muon-spin precession from μSR experimental data, where we observed the ratio between each precession component (10.6:3:1 for $M1_\mu$, $M2_\mu$, $M3_\mu$ respectively). We took into account this fact and the other positions then calculate the absolute difference between μSR and DFT results, and fit the data using the Gaussian function, we obtain that the best *U*-value for the La_2CuO_4 are 4.87(4) eV. By using this value, the calculated internal field is 429.7(12), 134.14(4), and 1,147.6(35) G for $M1_{DFT}$, $M2_{DFT}$, and $M3_{DFT}$. By comparing this value with the internal field value obtained from μSR experiment we measured the difference of internal field of 3.4 G (~1%), 38.2 (~40%), and 97.9 G (~8%) for M1, M2, and M3 respectively. All of the optimized muon positions and internal fields are summarized in Table

Table 3. Calculated internal field of $M1_{DFT}$, $M2_{DFT}$, and $M3_{DFT}$ obtained from DFT calculations by varying U.

	U (eV)												
	2	3	3.5	4	4.5	5	5.6	6	6.5	7	7.2	7.5	8
	Calculated magnetic moment without μ (μ_B)												
Magnetic moment	0.386	0.436	0.460	0.482	0.503	0.524	0.547	0.562	0.583	0.602	0.609	0.621	0.641
Muon position	Calculated internal fields, H_{DFT}^{Mi} (G)												
$M1_{DFT}$	336.35	376.01	384.85	391.51	429.28	446.36	450.22	471.50	474.90	491.08	503.83	507.16	523.10
$M2_{DFT}$	103.99	116.30	121.28	127.04	131.21	135.68	141.54	145.85	150.14	154.33	155.44	159.07	163.76
$M3_{DFT}$	888.06	990.60	1038.67	1077.89	1128.28	1169.74	1219.72	1241.02	1281.64	1322.98	1334.41	1364.36	1407.01

Summary and Recommendation

Throughout this thesis, we have confirmed that the supercell structure calculation is strictly required in order properly estimates the muon position inside the La_2CuO_4 structure. Two additional considerations are included in the form of the local deformation on the atomic structure and the spin states of the system. With the quantum correction of zero-point vibrational energy, we obtain the final position of muon that corresponds well to the latest μSR experimental study. The determination of specific *U*-value is another clear result for this study.

From the electrostatic potential calculation, we confirmed that the muon position is not strongly affected by the *U*-values which provides a good perspective if combined with the *U*-sensitive parameters like the Cu-spin states and the insulating gap. By adjusting the U-values and compare with the μSR experimental study, we obtain the specific *U*-value for La_2CuO_4 at 4.87(4) eV. This value also provides the best accuracy in terms of the insulating gap at 1.24(1) eV, Cu-spin states with the magnetic moment of 0.520(3) μ_B, furthermore it also the reproduce the μSR internal field. Making it a unique method to determine *U*-value and should provide an interesting discussion for many other strongly correlated systems in the future.

In the formalism of DFT with GGA PW91 as the exchange-correlation functional, the authors feel that the DFT study on the La_2CuO_4 can be considered to be finished. In the future, the author recommends:

1. Follows the same procedure to explore the stripe state in both hole doped and electron doped system.
2. Reveal the possible effects/differences of the chosen exchange-correlation functional by using the more modern function, SCAN.
3. Applies the method discussed on this doctoral study on other strongly correlated system. To further consolidate this method as one of the most accurate way to estimate the muon positions.

References

1. Carl D. Anderson and Seth H. Neddermeyer. (1936). Cloud Chamber Observation of Cosmic Rays at 4300 Meters Elevation and Near Sea-Level. *Physical Review* **50**, 263.
2. T. D. Lee and C. N. Yang. (1956). Question of Parity Conservation in Weak Interactions*. *Physical Review* **104**, 1.
3. R. L. Garwin, L. M. Lederman, and M. Weinrich. Observations of the Failure of Conservation of Parity and Charge Conjugation in Meson Decays: the Magnetic Moment of the Free Muon. *Physical Review* **105**, 1415.
4. K. Nagamine. (2003). *Introductory Muon Science*. Cambridge University Press.
5. A. A. Abrikosov and L. P. Gor'kov. (1961). On the Problem of the Knight Shift in Superconductor. *Soviet Physics: JETP* **12**, 2.
6. P. W. Anderson. (1987). The Resonating Valence Bond State in La_2CuO_4 and Superconductivity. *Science* **235**, 4793.
7. J. Hubbard. (1963). Electron Correlations in Narrow Energy Bands. *Proceeding of the Royal Society of London* **276**, 238-257.
8. F. C. Zhang and T. M. Rice. (1987). Effective Hamiltonian for the superconducting Cu oxides. *Physical Review B* **37**, 7.
9. J. M. Ginder, M. G. Roe, Y. Song, R. P. McCall, J. R. Gaines, and E. Ehrenfreundt. (1988). Photoexcitation in La_2CuO_4: 2-eV energy gap and long-lived defect states. *Physical Review B* **37**, 13.
10. N. Hasselmann, A. C. Neto, C. M. Smith. (2003). Spin-glass phase of cuprates. *Physical Review B* **69**, 1.
11. Q. Zhang, T. Cagin, W. A. Goddard III. (2006). The ferroelectric and cubic phases in BaTiO3 ferroelectrics are also antiferroelectric. *PNAS* **103**, 40.
12. T. Yokoo, K. Shibata and Y. Kuwano. (1985). Application of Pyroelectricity of $LiTaO_3$ for Infrared Detectors. *Japanese Journal of Applied Physics* **24**, 24-2.

13. W. Knafo, C. Meingast, A. V. Boris, P. Popovich, N. N. Kovaleva, P. Yordanov, A. Maljuk, R. K. Kremer, H. v. Löhneysen, and B. Keimer. (2009). Ferromagnetism and lattice distortions in the perovskite $YTiO_3$. *Physical Review B* **79**, 054431.
14. A. Buckley. (1999). Twin structures in tetragonal $SrTiO_3$: The ferroelastic phase transition and the formation of needle domains. *Journal of Applied Physics* **86**, 1653.
15. S. L. Bravina,N. V. Morozovsky,A. N. Morozovska,S. Gille,J.-P. Salvestrini &M. D. Fontana. (2007). Investigations of $LiNbO_3$ and $LiTaO_3$ Single Crystals for Pyroelectric Applications in the Wide Temperature Range. *Ferroelectrics* **353**, 1.
16. S. J. L. Billinge, G. H. Kwei and H. Takagi. (1994). Structural ground-state of La_2CuO_4 in the LTO phase: Evidence of local disorder. *Physica C: Superconductivity* **235-240**, 2.
17. P. Ganguly and C. N. R. Rao. (1973). Electron Transport Properties of Transition Metal Oxide Systems with the K_2NiF_4 Structure. *Material Research Bulletin* **8**, 405-412.
18. S. Uchida, H. Takagi, H. Yanagisawa, K. Kishio, K. Kitaza, K. Fueki and S. Tanaka. (1987). Electric and Magnetic Properties of La_2CuO_4. *Japanese Journal of Applied Physics* **26**, 4.
19. D. E. Rice and D. J. Buttrey. (1993). An X-Ray Diffraction Study of the Oxygen Content Phase Diagram of $La_2NiO_{4+\delta}$. *Journal of Solid State Chemistry* **205**, 1.
20. K. K. Singh, P. Ganguly and J. B. Goodenough. (1984). Unusual Effects of Anisotropic Bonding in Cu(ll) and Ni(ll) Oxides with K_2NiF_4 Structure. *Journal of Solid State Chemistry* **52**, 254-273.
21. D. Vaknin, S. K. Sinha, D. E. Moncton, D. C. Johnston, J. M. Newsam, C. R. Safinya, and H. E. King, Jr. (1987). Antiferromagnetism in La_2CuO_{4-y}. *Physical Review Letters* **58**, 2802.
22. B. Hitti, P. Birrer, K. Fischer, F. N. Gygax, E. Lippelt, H. Maletta, A. Schenck & M. Weber. (1991). Study of La_2CuO_4 and related compounds by μSR. *Hyperfine Interactions* **63**, 287-294.
23. T. Mcmullen, P. Jena and S. N. Khanna. (1991). Screening of a Positive Muon by Semion Gas. International Journal of Modern Physics B **5**, 1579.
24. SB Sulaiman, S Srinivas, N Sahoo, F Hagelberg, TP Das, E Torikai, K Nagamine. (1994). Theory of the location and associated hyperfine properties of the positive muon in La_2CuO_4. *Physical Review B* **49**, 9879.
25. G. Kresse and J. Furthmüller. (1996). Efficiency of ab-initio total energy calculations for metals and semiconductors using a plane-wave basis set. *Computational Materials Science* **6**, 1.
26. G. Kresse and J. Furthmüller. (1996). Efficient iterative schemes for ab initio total-energy calculations using a plane-wave basis set. *Physical Review B* **54**, 11169.
27. John P. Perdew, J. A. Chevary, S. H. Vosko, Koblar A. Jackson, Mark R. Pederson, D. J. Singh, and Carlos Fiolhais. (1993). Atoms, molecules, solids, and surfaces: Applications of the generalized gradient approximation for exchange and correlation. *Physical Review B* **46**, 6671.
28. E. Stilp, A. Suter, T. Prokscha, E. Morenzoni, H. Keller, B. M. Wojek, H. Luetkens, A. Gozar, G. Logvenov, and I. Božović. (2013). Magnetic phase diagram of low-doped $La_{2-x}Sr_xCuO_4$ thin films studied by low-energy muon-spin rotation. *Physical Review B* **88**, 064419.
29. V. G. Storchak, J. H. Brewer, D. G. Eshchenko, P. W. Mengyan, O. E. Parfenov, A. M. Tokmachev, P. Dosanjh and S. N. Barilo. (2014). Local magnetic order in La_2CuO_4 seen via μ^+SR spectroscopy. *Journal of Physics: Conference Series* **551**, 012024.
30. V. G. Storchak, J. H. Brewer, D. G. Eshchenko, P. W. Mengyan, O. E. Parfenov, A. M. Tokmachev and P. Dosanjh. (2016). Coupling of magnetic orders in La_2CuO_{4+x}. *Physical Review B* **94**, 134407.
31. A. Fujimori, E. Takayama-Muromachi, Y. Uchida, and B. Okai. (1987). Spectroscopic evidence for strongly correlated electronic states in La-Sr-Cu and Y-Ba-Cu oxides. *Physical Review B* **35**, 16.
32. T. Takahashi, F. Maeda, H. Arai, H. Katayama-Yoshida, Y. Okabe, T. Suzuki, S. Hosoya, A. Fujimori, T. Shidara, T. Koide, T. Miyahara, M. Onoda, S. Shamoto and M. Sato. (1987). Synchrotron-radiation photoemission study of the high-T, superconductor $YBa_2Cu_30_{7-\delta}$. *Physical Review B* **36**, 10.

APPENDIX

List of Presentation in International Conference:

1. M. R. Ramadhan *et al.*, Contribution of Quantum Effects on the Muon Site Calculation of La_2CuO_4. *The 4th Emallia Conference, Hokkaido Univ - Pusan Univ - RIKEN Symposium 2018*, Sapporo, Japan.
2. M. R. Ramadhan *et al*., Muon's Perturbation on the Local Spatial Distribution of Cu-Spin in La_2CuO_4 Simulated by Density Functional Theory Calculations. *The 12th International Conference on Materials and Mechanisms of Superconductivity and High Temperature Superconductors 2018*, Beijing, China.
3. M. R. Ramadhan *et al.*, A Revisit to the Ordered State of Cu-spins in La_2CuO_4 Simulated by DFT - Quantum Approach to Muon Sites. *Muon Spectroscopy User Meeting: Future Developments and Site Calculations 2018*, Abingdon, United Kingdom.
4. M. R. Ramadhan *et al.*, A Revisit to the Ordered State of Cu-Spins in La_2CuO_4 from the perspective of μSR and DFT. *The 5th International Symposium on Current Progress in Mathematics and Sciences 2019*, Depok, Indonesia.
5. M. R. Ramadhan *et al.*, Quantum Effects of Muon on the Electronic State of La_2CuO_4. *The 1st NCKU-RIKEN Joint Workshop, International Workshop on Topological Quantum Materials 2019*, Tainan, Taiwan.

List of Published Papers:

1. Effect of the Supercell's Size on Muon Positions Calculations of La_2CuO_4, M. R. Ramadhan et al., Mat. Sci. Forum, 966, 465-470, 2019.
2. Spin Alignment Studies on the Muon-Site Determination in La_2CuO_4, M. R. Ramadhan et al., Key Engineering Mat., 860, 154-159, 2020.
3. Estimation of the on-site Coulomb potential and covalent state in La_2CuO_4 by muon spin rotation and density functional theory calculations, M. R. Ramadhan et al., Phys. Rev. Research 4, 033044, 2022.

APPENDIX

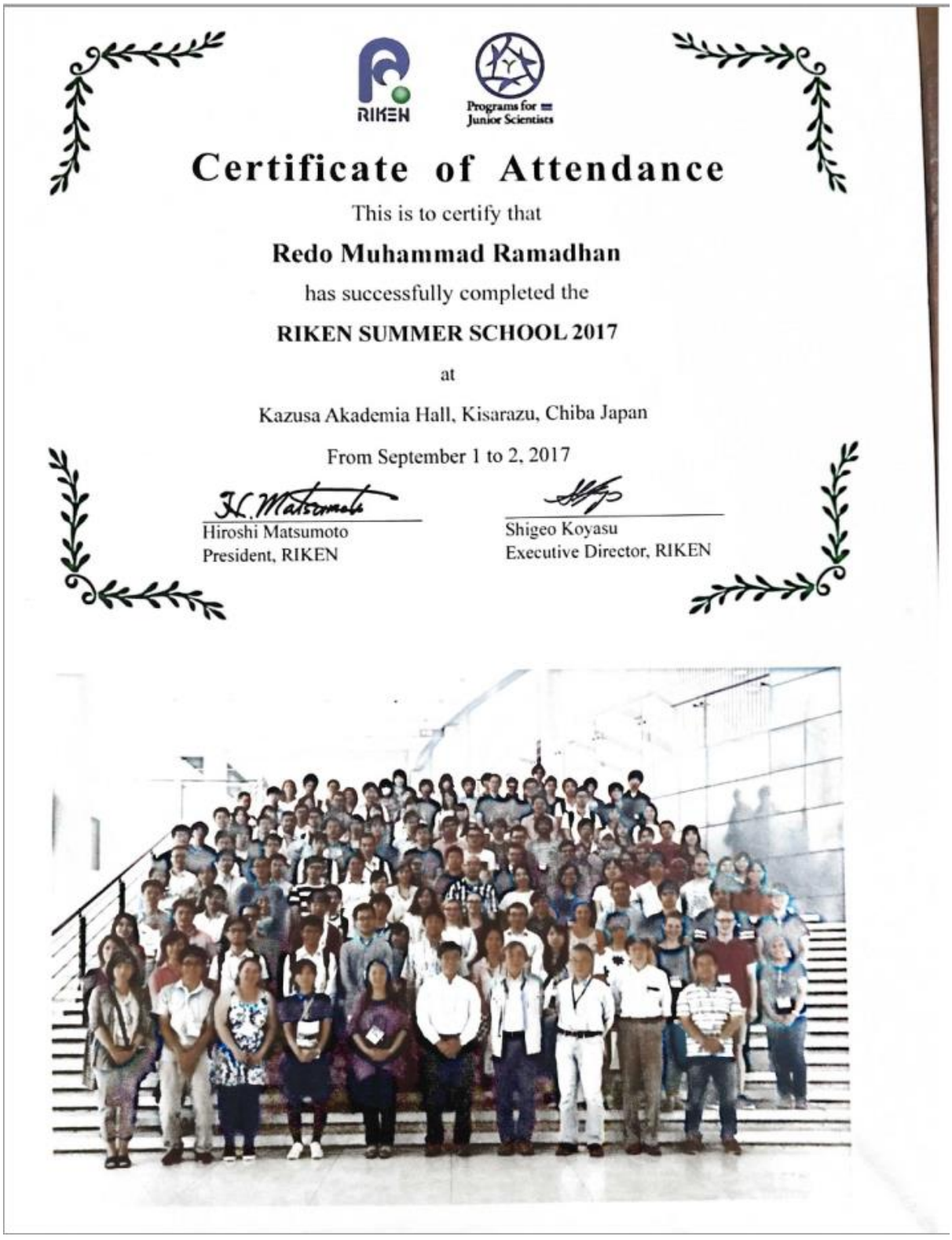

Figure A1. Certificate of Attendance in RIKEN Summer School 2017

APPENDIX

Figure A2. Certificate of Attendance in RIKEN Summer School 2018

APPENDIX

Figure A3. Physics Poster Prize in RIKEN Summer School 2017

Materials Science Forum
ISSN: 1662-9752, Vol. 966, pp 465-470
doi:10.4028/www.scientific.net/MSF.966.465

Submitted: 2018-12-04
Revised: 2019-05-15
Accepted: 2019-05-15
Online: 2019-08-06

Effects of the Supercell's Size on Muon Positions Calculations of La_2CuO_4

Muhammad Redo Ramadhan[1,2,a*], Irwan Ramli[1,3,4,b], Muhammad Darwis Umar[1,3,c], Suci Winarsih[1,2,d], Dita Puspita Sari[5,1,e] Azwar Manaf[2,f], Budhy Kurniawan[2,g], Mohamed Ismail Mohamed-Ibrahim[6,h], Shukri Sulaiman[6,7,i] and Isao Watanabe[1,2,3,6,7,j]

[1]Meson Science Laboratory, RIKEN Nishina Center, 2-1 Hirosawa, Wako 351-0198, Japan,

[2]Department of Physics, Faculty of Mathematics and Natural Sciences, Universitas Indonesia, Depok 16424, Indonesia,

[3]Muon Spin Resonance Laboratory, Department Condensed Matter Physics, Graduate School of Science, Hokkaido University, Sapporo 060-8010, Japan,

[4]Department of Physics, Faculty of Science, Universitas Cokroaminoto Palopo, Palopo 91921, Indonesia,

[5]Department of Regional Environment Systems, Graduate School of Engineering and Science, Shibaura Institute of Technology, Saitama City, Saitama 337-8570, Japan,

[6]Computational Chemistry and Physics Laboratory, Universiti Sains Malaysia, 11800, Malaysia,

[7]USM-RIKEN International Center for Ageing Science, School of Distance Education, Universiti Sains Malaysia, Pulau Pinang 11800, Malaysia.

[a*]redomuhammad.ramadhan@riken.jp, [b]irwan.ramli@riken.jp, [c]muhammad.umar@riken.jp, [d]suciwinarsih@riken.jp, [e]dita.puspita.sari.t1@shibaura-it.ac.jp, [f]azwar@ui.ac.id, [g]bkuru@fisika.ui.ac.id, [h]mi-mi@usm.my, [i]shukri@usm.my, [j]nabedon@riken.jp,

Keywords: Density functional theory, La_2CuO_4, muon's positions, supercell

Abstract. The outcome of density functional theory (DFT) technique within the supercell's framework of La_2CuO_4 (LCO) are reported. We evaluated local dipolar fields of muon's position inside LCO assuming dipolar interaction occurred by varying the supercell's size. We found out that the field on proposed muon's trapping positions was known to be not affected so much by the supercell's size and still fairly larger than the experimental data. Our results suggest that the inclusion of quantum effects of implanted muon and electronic spin are required to explain experimental data.

Introduction

La_2CuO_4 as the parent compound for the high-temperature superconducting cuprates has an insulating behavior and antiferromagnetism in the lower temperature region for its magnetic Cu atom. The antiferromagnetic behavior disappears with hole doping by substituting Sr or Ba in La atom, leading to the emergence of superconducting phase. This phenomenon was discovered by Bednorz and Müller in 1986 [1] and still remains a mystery to this date. La_2CuO_4 is also one of the Mott insulators, where it is known that the Hubbard's parameter U, and the exchange interaction J, between localized 3d electrons of Cu atom are important parameters to realize the electronic structure properly [2]. This consideration is also applied to another La-based superconductor to reveal the nature of the stripe which is common in the Cu-based superconductors [3].

Muon spin relaxation (μSR) measurements on LCO show the behavior of the antiferromagnetic long range ordered, where the existence of the coherent muon's precession was detected, and the local dipolar field of the muon's stopping position was known to be 400 – 430 G [4-7]. Powder neutron diffraction experiment by Vaknin *et al*. shows that LCO had an antiferromagnetic spin structure, where Cu spin has the magnetic moment of 0.5 μ_B and aligns in the CuO_2 plane along the b-axis [8]. Recent μSR experiments on the single crystal and thin film LCO reported the observation of another

muon's spin precession which experienced less local dipolar field at muon's positions of around 100 – 120 G [6, 7]. Although both μSR and neutron diffraction experiments sense the same Cu spin in LCO, it has not yet accomplished in explaining the local dipolar fields at muon's stopping positions by using antiferromagnetic spin structure proposed by the neutron diffraction experiment. This is because muon's stopping position has still not been precisely determined to explore the electronic structure surrounding the implanted muon in the antiferromagnetic ordered state. [9-13].

In this paper, we are developing the techniques to more precisely determine the stopping position of implanted muon in LCO by using density functional theory (DFT) technique. We have already shown the multi-muon states from the potential calculations in the one unit cell [9]. Furthermore, by taking into account the fact that the implanted muon can be regarded as a dilute charged impurity, calculation of the electronic structure within a supercell scheme with one muon is required. We have tested the supercell effect in previous study and pointed out its importance in the determination of muon stopping positions estimation in real materials [10]. Consequently, we have investigated the supercell size effect much more deeply and compare the calculation results among several supercells of different sizes.

Calculation Details

We have used DFT technique within the Kohn-Sham approach using the projector augmented-waves (PAW) formalism in Vienna *Ab-initio* Simulation Package (VASP) program [14, 15]. The exchange-correlation function that we used on this study is generalized gradient approximation (GGA 91) with the combination of the Hubbard's parameter U, and the exchange parameter J, to realistically describe the electron – electron correlation realized in Mott insulator. GGA is known to be an effective correlation function to describe electronic structure on the pure and doped LCO [3]. U and J were appointed to be 8 eV and 0.8 eV, respectively [3]. The antiferromagnetic spin structure from Vaknin *et al.* result was used to calculate the local fields at muon stopping positions [8]. For the initial parameter, we arranged Cu-spin's magnitude to be 0.5 μ_B and optimized it in our calculations to get a reasonable value of the magnetic moment of Cu spin.

Fig. 1 indicates the LCO crystal structure that was used in our calculations. This unit cell has an orthorhombic structure with *Pmmm* space group. Lattice parameters are a = 5.3568 Å, b = 5.4058 Å and c = 13.1432 Å, respectively [16]. This unit cell was used as the basis to form three different supercells to study the possible muon stopping positions. One is the formation of 2 × 2 × 1 which has

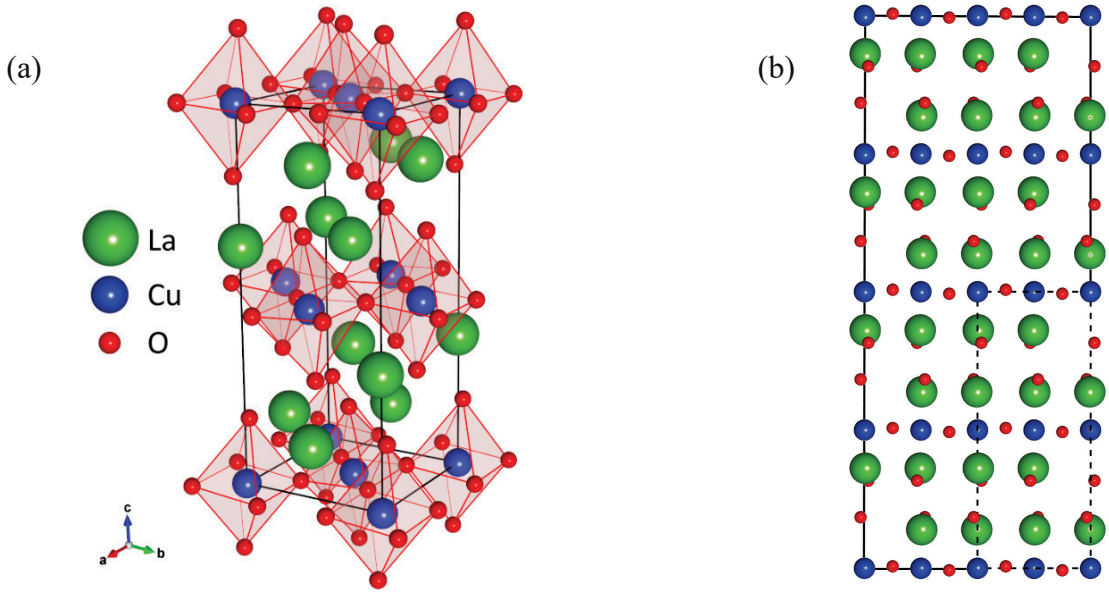

Fig. 1. La_2CuO_4 orthorhombic crystal structure (a) The 3-D picture of one-unit cell and (b) the side view of the 8-unit supercell with the formation of 2 × 2 × 2 viewed from the *b*-axis. Dashed line indicates unit cell's region in the 8-unit supercell. The data were visualized with VESTA [17].

4-unit cells. Second one is the formation of 3 × 3 × 1 which has 9-unit cells, while the third one is the formation of 2 × 2 × 2 which has 8-unit cells. Initially, we predicted the minimum potential position as reported in previous studies [9, 10]. The total free energy of supercell was achieved within the convergence accuracy of 1 x 10^{-5} eV. No lattice relaxation was considered to save the computational time and to make the comparison among the supercell models easier. Even in this case, we can simply compare the supercell size effect on local fields at muon's stopping positions. After determining the minimum potential which assumed as the initial stopping positions for implanted muons, we place one muon at each minimum position. Taking into consideration that there will be dipolar interactions, then we calculated the local field due to the surrounding Cu spins at each muon's positions.

The dipolar field at muon's positions coming from surrounding Cu spins was evaluated by the following equation:

$$H_{dip}(\vec{r}) = \sum_i \frac{1}{|\vec{r}-\vec{r}_i|}\left[3\left(\vec{\rho}_i^{S}\cdot(\vec{r}-\vec{r}_i)\right)\frac{(\vec{r}-\vec{r}_i)}{|\vec{r}-\vec{r}_i|^2}-\vec{\rho}_i^{S}\right], \quad (1)$$

where $\vec{\rho}_i^{S}$ is the magnetic moment of Cu spin and $|\vec{r}-\vec{r}_i|$ is the relative distance between the muon and Cu spins. The total dipolar field at muon's position, $H_{dip}(\vec{r})$, is obtained from the summation of the dipolar fields due to the surrounding Cu spins. For our calculations, we arranged the customized spherical region centered at the implanted muon with the radius of 50 Å. This customized spherical region is sufficient to converge the calculated dipolar field [9, 10].

Results and Discussions

To justify our calculation techniques for muon's stopping positions determination, the density of states (DOS) of each supercell was estimated without the muon. Fig. 2(a) shows the DOS calculation's result. The broken line in Fig. 2(a) indicates the Fermi energy level. The increase in the absolute values of DOS with increasing supercell size indicates the increase in the total number of electrons. DOS peak positions in all supercells did not change at all, suggesting that the supercell size did not alter the electronic structure of LCO in our calculations.

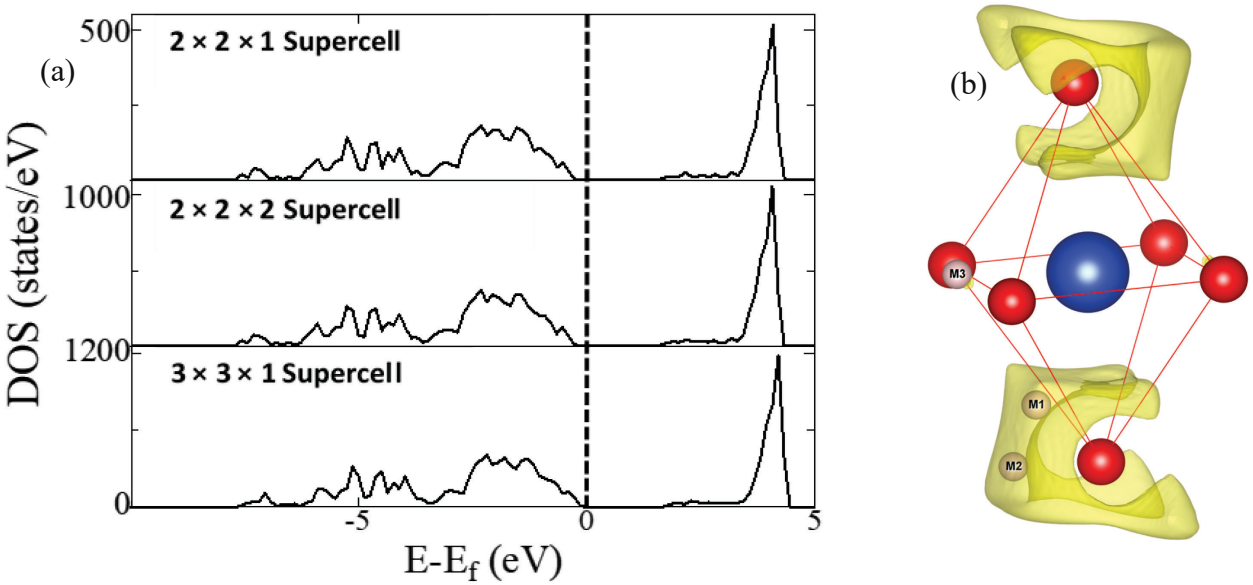

Fig. 2. (a) Density of states of La_2CuO_4 (LCO) for the 4-unit supercell, 8-unit supercell and 9-unit supercell. The broken line shows the Fermi energy level. (b) Potential minimum points estimated in our calculation by using unit cell labelled as M1, M2, and M3. The yellow area shows the iso-surface of 1000 meV from the minimum energy level.

Table 1. Distances between the muon and surrounding ions in of calculated supercells of La_2CuO_4.

	Cu (Å)			O (Å)		
	M1	**M2**	**M3**	**M1**	**M2**	**M3**
2 × 2 × 1	1.84013	2.70675	1.70474	1.07216	1.10277	1.29541
2 × 2 × 2	1.77366	2.76528	1.70474	1.08305	1.10872	1.29503
3 × 3 × 1	1.71259	2.70154	1.69230	1.08548	1.08354	1.29105

Furthermore, all the supercells had a large gap in Fermi energy level showing that insulating behavior is exist as expected from the Mott insulator. The gap that was determined from our calculations to be about ~ 1.9 eV for all three supercell models. This gap size was caused from the application of *U* and *J* parameter and is consistent with the result previously reported by other groups [18]. We have also optimized the magnitude of the effective Cu spin in our calculations and obtained that to be 0.61 μ_B/Cu-atom, which is slightly higher as compared to the value that was determined by neutron diffraction's experiments [8]. This value can be further adjusted by varying the values of *U* and *J*, as our used values of $U = 8$ eV and $J = 0.8$ V were determined by local spin density approximation (LSDA) study [2, 3] while we used GGA 91 which was more precise in general than LSDA for Mott insulators.

Fig. 2(b) shows electrostatic potential map in a unit-cell as estimated from our DFT technique on the iso-surface level of 1000 meV from the ground state. For the convenience, we labelled M1, M2 and M3 to shows the observed minimum positions for LCO electrostatic potential map. Both M1 and M2 are located on the vicinity of apical oxygen, while M3 is positioned almost in between planar oxygen of the CuO_6 octahedra. Table 1 show distances between each muon's position to the surrounding Cu and the nearest O ions. Variations in the distance due to the size of supercells are not so significant and within the order of a couple of percent. This suggests that the supercell size does not alter the muon's position significantly. By treating M1, M2 and M3 to be a muon stopping positions, we simply calculated local fields from surrounding Cu spins at each muon's positions by using Eq. 1. Table 2 summarizes the results. From our calculations, it is clear that the supercell size did not give any large effects on the local dipolar field at those muon positions. This can be simply understood that muon's position and relative distances to Cu spin did not change so much even in different supercell sizes.

We have compared our calculation results with experimental data to evaluate our current calculation's initial parameters. Two muon stopping positions are recognized experimentally from previous μSR investigations. One is the major one which is observed in any LCO samples and feels the local dipolar field of 400–430 G [4-7]. The other one is observed only in thin films and single crystals and feels less local field of 100–120 G [6, 7]. Those experimental data are smaller than those that we have calculated from our DFT technique. It means that we were required to consider more factors which can reduce the estimated local field effectively. Our former muon's position investigations faced a similar issue and it is suggested to take into account quantum effects induced by the implanted muon to both local crystal and the spin structure, and also the Zero-Point energy of the implanted muon itself [19, 20]. These quantum effects were recently examined and suggested to be effective to simulate the μSR data [21]. We believe those quantum effects are the key points and mandatory to obtain more information on muon's stopping positions inside the LCO system.

Table 2. Dipolar fields at three muon stopping positions in La_2CuO_4 which are estimated from our DFT technique by varying the size of supercell model.

Supercell Sizes	**2 × 2 × 1 cells**			**3 × 3 × 1 cells**			**2 × 2 × 2 cells**		
Muon Positions	**M1**	**M2**	**M3**	**M1**	**M2**	**M3**	**M1**	**M2**	**M3**
Dipolar Field (G)	1037	322	2667	1044	324	2972	1163	300	2667

Summary

We have carried out density functional theory calculations on La_2CuO_4, to estimate muon's position and dipolar fields at proposed positions. We found that there are three muon's possible positions in the LCO system from our calculation results although only two stopping positions were recognized experimentally from previous muon spin relaxation (μSR) investigations. We examined the effects of supercell's size to estimate muon's position and the local fields. Almost no significant discrepancies were confirmed, and the supercell size effect was not apparent in our calculations. We observed that the dipolar fields at muon stopping positions were still higher than those obtained experimentally. More precise calculations by taking into account the quantum effects which are induced by the implanted muon and also the muon's own quantum effects are required to be properly considered in future studies.

Acknowledgement

The authors gratefully acknowledge the supports from the International Program Associate (IPA) RIKEN, Japan and also for the allocation of computing resources on the Big Wave HOKUSAI Massive Parallel Computer (Project number G18022) from the RIKEN Advanced Center for Computing and Communication (ACCC). Two of us (SS and MIMI) would like to acknowledge the financial support by Universiti Sains Malaysia through a Research University Grant (Grant No. 1001/PJJAUH/870037). This study is supported by the Bilateral Program of Japan Society for the Promotion of Science.

References

[1] J. G. Bednorz and K. A. Muller, Possible high T_c superconductivity in the Ba-La-Cu-O system, Z. Physik B 64 (1986) 189-193.

[2] V. I. Anisimov and O. Gunnarsson, Density-functional calculation of effective Coulomb interaction in metals, Phys. Rev. B 43 (1991) 7570.

[3] S. Pesant and M. Côté, DFT + U study of magnetic order in doped La_2CuO_4 crystals, Phys. Rev. B 84 (2011) 085104.

[4] J. I. Budnick, A. Golnik, Ch. Niedermayer, E. Recknagel, M. Rossmanith, A. Weidinger, B. Chamberland, M. Filipkowski, D. P. Yang, Observation of magnetic ordering in La_2CuO_4 by muon spin spectroscopy, Phys. Lett. A 124 (1987) 103-106.

[5] Y. J. Uemura, Muon spin relaxation studies on high-T_c superconductors and related antiferromagnet (invited), J. App. Phys 64 (1988) 6087.

[6] E. Stilp, A. Suter, T. Prokscha, E. Morenzoni, H. Keller, B. M. Wojek, H. Luetkens, A. Gozar, G. Logvenov, and I. Bozovic, Magnetic phase diagram of low-doped $La_{2-x}Sr_xCuO_4$ thin films studied by low-energy muon-spin rotation, Phys. Rev. B 88 (2013) 064419.

[7] V. G. Storchak, J. H. Brewer, D. G. Eshchenko, P. W. Mengyan, O. E. Parfenov, A. M. Tokmachev, P. Dosanjh and S. N. Barilo, Local magnetic order in La_2CuO_4 seen via μ^+SR spectroscopy, J. Phys.: Conf. Ser. 551 (2014) 012024.

[8] D. Vaknin, S. K. Sinha, D. E. Moncton, D. C. Johnston, J. M. Newsam, C. R. Safinya, and H. E. King, Jr., Antiferromagnetism in La_2CuO_{4-y}, Phys. Rev. Lett. 58 (1987) 2802.

[9] B Adiperdana. A. Dharmawan, R.E. Siregar, I. Watanabe, K. Ohishi, Y. Ishii, T. Suzuki, T. Kawamata, Risdiana, R. Sheuermann, K. Sedlak, Y. Tomioka, T. Waki, Y. Tabata, and H. Nakamura, Muon Sites Estimation in La_2CuO_4 and A New Vanadium Cluster Compound, $V_4S_9Br_4$, using electronic and dipole field calculations, Phys. Procedia 30 (2012) 109.

[10] B. Adiperdana, E. Suprayoga, N. Adam, Mohm-Tajudin S.S., Rozlan A.F., S. Sulaiman, M.I. Mohamed-Ibrahim, T. Kawamata, T. Adachi, I.A. Dharmawan, R.E. Siregar, Y. Koike, and I. Watanabe, An Effect of the Super-Cell Calculation on Muon Positions and Local Deformations of Crystal Structure in La_2CuO_4, J. Phys. Conf. Ser. 551 (2014) 012051-1-6.

[11] B. Hitti, P. Birrer, K. Fischer, F. N. Gygax, E. Lippelt, H. Maletta, A. Schenck and M. Weber, Study of La_2CuO_4 and related compounds by μSR, Hyperfine Interact. 63 (1990) 287-294.

[12] E. Torikai, K. Nagamine, H. Kitazawa, I. Tanaka, H. Kojima, S. B. Sulaiman, S. Srinivas, T. P. Das, Behavior of positive muons in high Tc superconductors $La_{2-x}Sr_xCuO_4$, Hyperfine Interact. 79 (1993) 921.

[13] S. B. Sulaiman, N. Sahoo, S. Srinivas, F. Hagelberg, T. P. Das, E. Torikai, K. Nagamine, Theory of location and associated hyperfine properties of the positive muon in La_2CuO_4, Hyperfine Interact. 84 (1994) 87-103.

[14] G. Kresse and J. Furthmüller, Efficient iterative schemes for ab initio total-energy calculations using a plane-wave basis set, Phys. Rev. B 54 (1996) 11169.

[15] G. Kresse and J. Furthmüller, Efficiency of ab-initio total energy calculations for metals and semiconductors using a plane-wave basis set, Comp. Mater. Sci. 6 (1996) 15-50.

[16] M. Reehuis, C. Ulrich, K. Prokeš, A. Gozar, G. Blumberg, S. Komiya, Y. Ando, P. Pattison, and B. Keimer, Crystal structure and high-field magnetism of La_2CuO_4, Phys. Rev. B 73 (2006). 144513.

[17] K. Momma and F. Izumi, VESTA 3 for three-dimensional visualization of crystal, volumetric and morphology data, J. Appl. Crystallogr. 44 (2011) 1272-1276.

[18] J. M. Grinder, M. G. Roe, Y. Song, R. P. McCall, J. R. Gaines, and E. Ehrenfreund, Photoexcitations in La_2CuO_4: 2-eV energy gap and long-lived defect states, Phys. Rev. B 37 (1988) 7506.

[19] S.S. Mohd-Tajudin, S.N.A. Ahmad, D.F. Hasan-Baseri, E. Suprayoga, N. Adam, Rozlan A.F., S. Sulaiman, M.I. Mohamed-Ibrahim, and I. Watanabe, An Investigation of Muon Sites in $YBa_2Cu_3O_6$ by using Density Functional Theory, J. Phys. Conf. Ser. 551 (2014) 012052-1-6.

[20] E. Suprayoga, A.A. Nugroho, A.O. Polyakov, T.T.M. Palstra, and I. Watanabe, Search for Potential Minimum Positions in Metal-Organic Hybrids, $(C_2H_5NH_3)_2CuCl_4$ and $(C_6H_5CH_2CH_2NH_3)_2CuCl_4$, by Using Density Functional Theory, J. Phys. Conf. Ser. 551 (2014) 012054-1-6.

[21] E. Suprayoga, A. A. Nugroho, D. Onggo, A. O. Polyakov, T. T. M. Palstra, and I. Watanabe, 3D long-range magnetic ordering in $(C_2H_5NH_3)_2CuCl_4$ compound revealed by internal magnetic field from muon spin rotation and first principal calculation, Physica B: Cond. Matt. 545 (2018) 76-79.

Key Engineering Materials
ISSN: 1662-9795, Vol. 860, pp 154-159
doi:10.4028/www.scientific.net/KEM.860.154

Submitted: 2019-11-30
Revised: 2020-04-04
Accepted: 2020-05-01
Online: 2020-08-25

Spin Alignment Studies on the Muon-Site Determination in La_2CuO_4

Muhammad Redo Ramadhan[1,2,3,a], Irwan Ramli[1,3,4,b], Dita Puspita Sari[5,1,c], Budhy Kurniawan[2,d*], Azwar Manaf[2,e*], Mohamed Ismail Mohamed-Ibrahim[6,f], Shukri Sulaiman[6,7,g] and Isao Watanabe[1,2,3,6,7,h]

[1]Meson Science Laboratory, RIKEN Nishina Center, 2-1 Hirosawa, Wako 351-0198, Japan,

[2]Department of Physics, Faculty of Mathematics and Natural Sciences, Universitas Indonesia, Depok 16424, Indonesia,

[3]Muon Spin Resonance Laboratory, Department Condensed Matter Physics, Graduate School of Science, Hokkaido University, Sapporo 060-8010, Japan,

[4]Department of Physics, Faculty of Science, Universitas Cokroaminoto Palopo, Palopo 91921, Indonesia,

[5]Department of Regional Environment Systems, Graduate School of Engineering and Science, Shibaura Institute of Technology, Saitama City, Saitama 337-8570, Japan,

[6]Computational Chemistry and Physics Laboratory, School of Distance Education, Universiti Sains Malaysia, 11800, Malaysia,

[7]USM-RIKEN International Center for Ageing Science (URICAS), School of Distance Education, Universiti Sains Malaysia, Pulau Pinang 11800, Malaysia.

[a]redoramadhan70@gmail.com, [b]irwan.ramli@riken.jp, [c]dita.puspita.sari.t1@shibaura-it.ac.jp, [d]budhy.kurniawan@sci.ui.ac.id, [e*]azwar@ui.ac.id, [f]mi-mi@usm.my, [g]shukri@usm.my, [h]nabedon@riken.jp

Keywords: spin alignment, La_2CuO_4, Density Functional Theory, Muon-Site

Abstract. Here we report spin-alignment contributions to muon coordinate calculated utilizing density functional theory (DFT) calculation. We estimated four different antiferromagnetic (AF) spin alignments in La_2CuO_4. We observed small changes by adjusting spin configurations in DFT calculations. Cu-spin value of 0.61 μB is constant in all calculations. The insulating gap of 1.9 eV is unchanged in all configurations. Muon coordinate was defined as the most minimum energy in atomic potential distribution. By assuming that Cu-spin is a point dipole for each atom, internal fields for muon were calculated and compared to known experimental results.

Introduction

Due to rising of interests caused by discovery of high-T_C superconductivity in the late 80's [1], La_2CuO_4 as mother compound of those systems is subjected to wide variation of measurements. This system has insulating characteristic, coupled with antiferromagnetic state originated from the superexchange between neighboring Cu atoms, mediated by O. The aforementioned state will vanish accordingly with holes addition process by replacing a part of (La) ion with Sr and Ba ions and superconducting state appears, signifying the close relation between superconductivity and magnetic state. Antiferromagnetic in La_2CuO_4 was firstly observed from neutron diffraction technique [2]. The magnetic configuration was formed by an alternating Cu-spins on each octahedral arrangement between one Cu with 4 planar and 2 apical O. In their experiment, it was determined that value for Cu-spin is approximately ~0.5 μ_B.

Another experiment that successfully observed the AF-LRO is by utilizing muon spin rotation/relaxation (μSR) technique, which uses muon as local magnetic probe. μSR showed a coherent precession of muon spin, realizing a long-range behavior in this system [3,4]. From muon precession frequency, the field that is experienced by muon was calculated at around 400 G [3-6]. However, there is discrepancy with neutron technique, where spin configuration given from neutron

experiment cannot explain the internal field value calculated in muon experiments. One strong reason of these differences is the vagueness of muon coordinates in La_2CuO_4 [7-11].

To get additional insight of this discrepancy, we applied density functional theory (DFT) calculation for La_2CuO_4 structure and considering on-site Coulomb repulsion energy, *U*, on each Cu to get appropriate electronic ground states. Then, we calculated muon coordinates based on its atomic potential. This DFT+ *U* method has been known producing good results for both La_2CuO_4 [12] and hole-doped superconducting system [13]. Four La_2CuO_4 spin configurations were evaluated, one configuration was suggested based on neutron studies [2], while three possible spin configurations were evaluated in muon studies by Stilp *et al.* [5]. Here, we reveal possible spin alignment contributions of muon sites and their immediate effects to internal field values.

Calculation Details

VASP software was utilized for DFT calculation [14, 15]. GGA PW91 functional was chosen together with addition of *U*-value realizing appropriate electronic ground states for La_2CuO_4 structure. Based on our past studies [16,17], we observe a minimal change on muon coordinates with respect to variation of *U* and supercell size, aside from the obvious changes in Cu-spin that relies on given *U*-value. Thus, both parameters were held constant. Accordingly, *U*-value was fixed at 7.2 eV, to get the proper insulating energy gap as observed from the experiment [20], and supercell containing 4-unit cells in $2 \times 2 \times 1$ formation was utilized for all calculations.

Figure 1 depicts La_2CuO_4 magnetic configurations labelled as SS-A, SS-B, SS-C and SS-D. The unit cell structure has orthorhombic structure with space group *Pmmm*, consisting of two alternating layers of CuO_4 plane. Lattice parameters for unit cell were fixed at a = 5.3568 Å, b = 5.4058 Å and c = 13.1432 Å [18]. This unit cell is basis structure to form the $2 \times 2 \times 1$ supercell structure. SS-A is defined as default (010) configuration, as shown in neutron study [2]. In SS-B, we switch the direction of spin to (110) direction. In SS-C, and SS-D, we set lower layer of CuO_4 (red arrow) to (010) direction, while switching upper layer of CuO_4 (green arrow) to (100) and (110) direction respectively. All structures were optimized with energy convergence criterion of 10^{-4} eV. Lattice and volume relaxations were not considered avoiding massive computational times required for supercell calculations. Possible muon coordinates were calculated from its atomic electrostatic potential. We calculated internal field value on those positions assuming dipole interaction between muon and spin at Cu. The field is calculated using below equation:

$$H_{dip}(\vec{r}) = \sum_i \frac{1}{|\vec{r}-\vec{r}_i|}\left[3\left(\vec{\rho}_i^S \cdot (\vec{r}-\vec{r}_i)\right)\frac{(\vec{r}-\vec{r}_i)}{|\vec{r}-\vec{r}_i|^2} - \vec{\rho}_i^S\right], \quad (1)$$

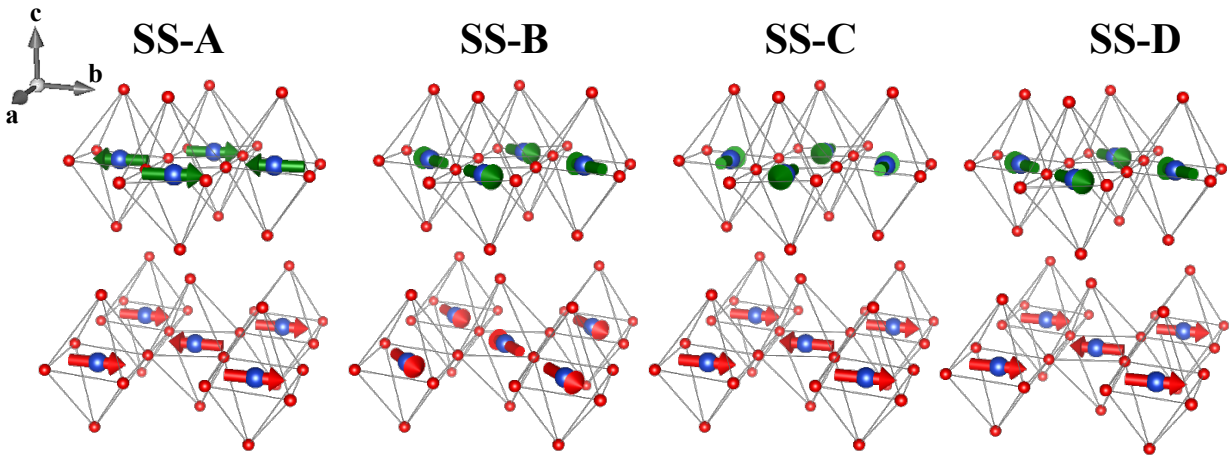

Fig. 1. La_2CuO_4 AF-spin configurations drawn in CuO_6 octahedra. Red and green arrows indicate the same Cu-spin on the different layer of supercell. The figure was visualized with VESTA [19].

$\vec{\rho}_i^S$ is Cu-spin value, while $|\vec{r} - \vec{r}_i|$ is distance from Cu atom to muon. Internal field for muon, $H_{dip}(\vec{r})$, was defined as addition of all contributing Cu-spin to muon coordinate. We utilized the Lorentzian sphere with radius of 100 Å with muon in center to follow realistic experimental conditions. The chosen radius was sufficient to get convergence in summation process of $H_{dip}(\vec{r})$ [8, 9].

Results and Discussions

Density of state (DOS) for each spin configuration is shown on Fig. 2. The striped line shows Fermi level as calculated from DFT and normalized to 0 eV. Electrons in Cu 3*d*-orbital occupy both the conduction and valence bands separated by *U*. The O 2*p*-orbital electrons occupy the upper region of valence band near Fermi level. The energy gap was found constant at 1.9 eV in all calculations. This indicates that electronic ground states do not changed at different AF spin configurations. This is consistent with energy gap value observed experimentally in the past study [20]. For electrostatic potential calculation, we do not observe any significant changes with different AF-spin configuration. Three muon coordinates were observed for all spin configurations. We labelled those coordinates as M1, M2, M3 based on its potential energy value. These muon coordinates are consistent with our past study [16]. Table 1 describes three key parameters. All spin configurations have similar value of spin, the spin alignment of SS-A and SS-C have 0.61 μ_B/Cu, while SS-B and SS-D have 0.609 μ_B/Cu. These values are slightly larger compared to neutron studies [2]. In the case of SS-C, even though we reversed spin direction to *x*-axis (100), Cu-spin value is still retained. From the total energy perspective, SS-B is the most stable structure, consistent with recent neutron study which reported that slight tilting of Cu-spin direction is favorable compared to previously proposed one [2,18].

The electrostatic potential from DFT calculations shows a slight variation between M1, M3 coordinates while relatively constant for M2 coordinates. Those slight changes are likely exists as consequence of changing the spin configurations, since both coordinates (M1, M3) are closer to Cu-atom. This result indicates that different AF spin configurations do not affect muon coordinates significantly.

To confirm this, we calculate $H_{dip}(\vec{r})$ at M1, M2, M3 coordinates for all spin configurations by employing Eq. 1. Table 2 show the summarized results. We confirmed slight variations of $H_{dip}(\vec{r})$

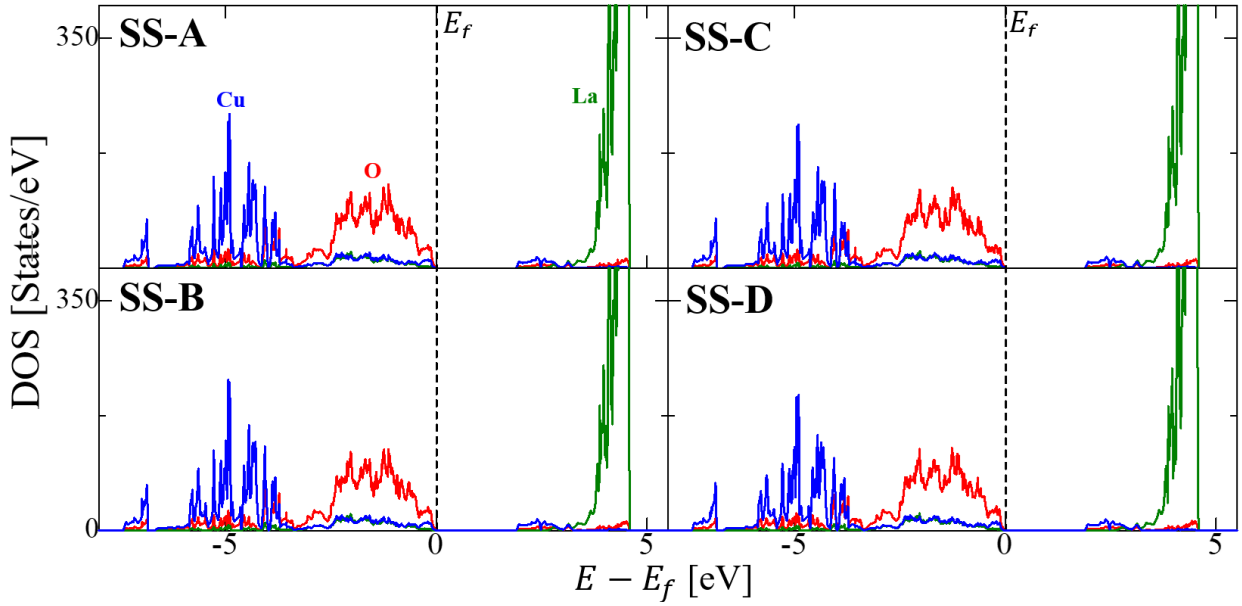

Fig. 2. (a) Density of state of La_2CuO_4 in 4 different spin configurations. Broken lines show the Fermi level normalized to 0 eV. Blue, red and green lines indicate Cu, O, and La atom's electronic states respectively.

Table 1. Absolute Cu-spin values, potential energy values, and distance of muon to Cu in respect to AF-spin configurations.

	Abs. Cu-spin [μ_B]			Potential Energy [eV]			Distance to Cu ion [Å]		
	x	y	z	M1	M2	M3	M1	M2	M3
SS-A	0.002	0.610	0.005	11.262	11.140	10.350	1.840	2.707	1.705
SS-B	0.432	0.430	0.000	11.267	11.143	10.355	1.840	2.707	1.708
SS-C1	0.001	0.610	0.000	11.263	11.141	10.347	1.840	2.707	1.708
SS-C2	0.610	0.002	0.000						
SS-D1	0.003	0.610	0.000	11.253	11.140	10.358	1.840	2.707	1.708
SS-D2	0.431	0.431	0.000						

by utilizing different spin configurations. From the known experimental results, two muon coordinates were observed from thin-film and single crystal [5,6]. One coordinate is recognized as largest contributor with $H_{dip}(\vec{r})$ at ~400 G and second one has smaller $H_{dip}(\vec{r})$ at ~100 G. The SS-A configurations, showed nearly 3 times larger values for M1, M2 coordinates. Interestingly, $H_{dip}(\vec{r})$ is reduced slightly for SS-C (~5 % for M1, ~13 % for M2). However, these values are still too large compared to experimental results [3-6]. Thus, further considerations are necessary to accurately calculates muon electronic states. One possibility is to include quantum effect given by muon to neighboring Cu-spins and atomic potential, which we believed as important clue that is missing from muon coordinate studies.

Table 2. Internal fields at three muon coordinates in La_2CuO_4.

	Internal Field [Gauss]		
	M1	M2	M3
SS-A	1037	322	2667
SS-B	1103	370	2289
SS-C	981	278	1904
SS-D	1100	379	2325

Summary

We performed density functional theory (DFT) calculation for La_2CuO_4 structure. The Coulomb repulsion energy, *U*, was explicitly included. To study possible spin configuration effect, we set four different antiferromagnetic (AF) configurations. No significant changes were obtained in terms of electronic ground states at different spin configurations. All spin configurations showed the AF alignment with 0.61 μ_B/Cu and 1.9 eV insulating gap. Three possible muon coordinates were proposed, while two muon coordinates were detected experimentally. Slight variations were obtained in electrostatic potential and internal fields. Our result indicates that electronic ground states at muon coordinates are slightly affected by Cu-spin configurations. Our calculated internal fields are still larger compared to experimental results. Further investigations by considering quantum effect caused by muon themselves are needed to accurately calculates muon coordinate.

Acknowledgement

The authors gratefully acknowledge the supports from the International Program Associate (IPA) RIKEN, Japan and also for the allocation of computing resources on the Big Wave HOKUSAI Massive Parallel Computer (Project number G19007) from the RIKEN Advanced Center for Computing and Communication (ACCC). Two of us (SS and MIMI) would like to acknowledge the financial support by Universiti Sains Malaysia through a Research University Grant (Grant No. 1001/PJJAUH/870037). This study is supported by the Bilateral Program of Japan Society for the Promotion of Science.

References

[1] J.G. Bednorz, K.A. Muller, Possible high T_c superconductivity in the Ba-La-Cu-O system, Z. Physik B 64 (1986) 189–193.

[2] D. Vaknin, S.K. Sinha, D.E. Moncton, D.C. Johnston, J.M. Newsam, C.R. Safinya, H.E. King, Jr., Antiferromagnetism in La_2CuO_{4-y}, Phys. Rev. Lett. 58 (1987) 2802.

[3] J.I. Budnick, A. Golnik, Ch. Niedermayer, E. Recknagel, M. Rossmanith, A. Weidinger, B. Chamberland, M. Filipkowski, D.P. Yang, Observation of magnetic ordering in La_2CuO_4 by muon spin spectroscopy, Phys. Lett. A 124 (1987) 103–106.

[4] Y.J. Uemura, Muon spin relaxation studies on high-T_c superconductors and related antiferromagnet (invited), J. App. Phys 64 (1988) 6087.

[5] E. Stilp, A. Suter, T. Prokscha, E. Morenzoni, H. Keller, B. M. Wojek, H. Luetkens, A. Gozar, G. Logvenov, I. Bozovic, Magnetic phase diagram of low-doped $La_{2-x}Sr_xCuO_4$ thin films studied by low-energy muon-spin rotation, Phys. Rev. B 88 (2013) 064419.

[6] V.G. Storchak, J.H. Brewer, D.G. Eshchenko, P. W. Mengyan, O. E. Parfenov, A.M. Tokmachev, P. Dosanjh, S.N. Barilo, Local magnetic order in La_2CuO_4 seen via μ^+SR spectroscopy, J. Phys.: Conf. Ser. 551 (2014) 012024.

[7] B. Adiperdana. A. Dharmawan, R.E. Siregar, I. Watanabe, K. Ohishi, Y. Ishii, T. Suzuki, T. Kawamata, Risdiana, R. Sheuermann, K. Sedlak, Y. Tomioka, T. Waki, Y. Tabata, H. Nakamura, Muon sites estimation in La_2CuO_4 and a new vanadium cluster compound, $V_4S_9Br_4$, using electronic and dipole field calculations, Phys. Procedia 30 (2012) 109.

[8] B. Adiperdana, E. Suprayoga, N. Adam, Mohm-Tajudin S.S., Rozlan A.F., S. Sulaiman, M.I. Mohamed-Ibrahim, T. Kawamata, T. Adachi, I.A. Dharmawan, R.E. Siregar, Y. Koike, I. Watanabe, An effect of the super-cell calculation on muon positions and local deformations of crystal structure in La_2CuO_4, J. Phys. Conf. Ser. 551 (2014) 012051.

[9] B. Hitti, P. Birrer, K. Fischer, F. N. Gygax, E. Lippelt, H. Maletta, A. Schenck, M. Weber, Study of La_2CuO_4 and related compounds by μSR, Hyperfine Interact. 63 (1990) 287–294.

[10] E. Torikai, K. Nagamine, H. Kitazawa, I. Tanaka, H. Kojima, S. B. Sulaiman, S. Srinivas, T. P. Das, Behavior of positive muons in high Tc superconductors $La_{2-x}Sr_xCuO_4$, Hyperfine Interact. 79 (1993) 921–927.

[11] S.B. Sulaiman, N. Sahoo, S. Srinivas, F. Hagelberg, T.P. Das, E. Torikai, K. Nagamine, Theory of location and associated hyperfine properties of the positive muon in La_2CuO_4, Hyperfine Interact. 84 (1994) 87–103.

[12] V.I. Anisimov, O. Gunnarsson, Density-functional calculation of effective Coulomb interaction in metals, Phys. Rev. B 43 (1991) 7570–7574.

[13] S. Pesant, M. Côté, DFT+U study of magnetic order in doped La_2CuO_4 crystals, Phys. Rev. B 84 (2011) 085104.

[14] G. Kresse, J. Furthmüller, Efficient iterative schemes for ab initio total-energy calculations using a plane-wave basis set, Phys. Rev. B 54 (1996) 11169.

[15] G. Kresse, J. Furthmüller, Efficiency of ab-initio total energy calculations for metals and semiconductors using a plane-wave basis set, Comp. Mater. Sci. 6 (1996) 15–50.

[16] M.R. Ramadhan, I. Ramli, M.D. Umar, S. Winarsih, D.P. Sari, A. Manaf, B. Kurniawan, M.I. Mohamed-Ibrahim, S. Sulaiman, I. Watanabe, Effects of the supercell's size on muon positions calculations of La_2CuO_4, Mat. Sci. Forum 966 (2019) 465–470.

[17] I. Ramli, S.S. Mohd-Tajudin, M. R. Ramadhan, D. P. Sari, S. Sulaiman, M. I. Mohamed-Ibrahim, B. Kurniawan, I. Watanabe, Magnetic properties of $YBa_2Cu_3O_6$ studied by density functional theory calculations, Mat. Sci. Forum 966 (2019) 257–262.

[18] M. Reehuis, C. Ulrich, K. Prokeš, A. Gozar, G. Blumberg, S. Komiya, Y. Ando, P. Pattison, B. Keimer, Crystal structure and high-field magnetism of La_2CuO_4, Phys. Rev. B 73 (2006) 144513.

[19] K. Momma, F. Izumi, VESTA 3 for three-dimensional visualization of crystal, volumetric and morphology data, J. Appl. Crystallogr. 44 (2011) 1272–1276.

[20] J. M. Grinder, M. G. Roe, Y. Song, R. P. McCall, J. R. Gaines, E. Ehrenfreund, Photoexcitations in La_2CuO_4: 2-eV energy gap and long-lived defect states, Phys. Rev. B 37 (1988) 7506.

Estimation of the on-site Coulomb potential and covalent state in La_2CuO_4 by muon spin rotation and density functional theory calculations

Muhammad Redo Ramadhan,[1,2,*] Budi Adiperdana,[1,3] Irwan Ramli,[1,4,†] Dita Puspita Sari,[1,5,‡] Anita Eka Putri,[1,2] Utami Widyaiswari,[1,2,4] Harison binti Rozak,[1,6,§] Wan Nurfadhilah Zaharim,[1,6,‖] Azwar Manaf,[2] Budhy Kurniawan,[2,¶] Mohamed Ismail Mohamed-Ibrahim,[6] Shukri Sulaiman,[1,6,‖] Takayuki Kawamata,[7,#] Tadashi Adachi,[8] Yoji Koike,[7] and Isao Watanabe[1,2,3,4,5,6,**]

[1]*Meson Science Laboratory, RIKEN Nishina Center, 2-1 Hirosawa, Wako, Saitama 351-0198, Japan*
[2]*Department of Physics, Universitas Indonesia, Depok 16424, Indonesia*
[3]*Department of Physics, Universitas Padjajaran, Sumedang 45363, Indonesia*
[4]*Department of Condensed Matter Physics, Hokkaido University, Sapporo 060-8010, Japan*
[5]*Department of Physics, Osaka University, Osaka 560-0043, Japan*
[6]*Computational Chemistry and Physics Laboratory, School of Distance Education, Universiti Sains Malaysia, Pulau Pinang 11800, Malaysia*
[7]*Department of Applied Physics, Tohoku University, Sendai 980-8579, Japan*
[8]*Department of Engineering and Applied Sciences, Sophia University, Tokyo 102-8554, Japan*

(Received 3 October 2020; revised 22 March 2022; accepted 17 June 2022; published 15 July 2022)

The on-site Coulomb potential, U, and the covalent state of electronic orbitals play key roles for the Cooper pair symmetry and exotic electromagnetic properties of high-T_c superconducting cuprates. In this paper, we demonstrate a way to determine the value of U and present the whole picture of the covalent state of Cu spins in the mother system of the La-based high-T_c superconducting cuprate, La_2CuO_4, by combining the muon spin rotation (μSR) and the density functional theory (DFT) calculation. We reveal local deformations of the CuO_6 octahedron followed by changes in Cu-spin distributions caused by the injected muon. Adjusting the DFT and μSR results, U and the minimum charge-transfer energy between the upper Hubbard band and the O $2p$ band were optimized to be 4.87(4) and 1.24(1) eV, respectively.

DOI: 10.1103/PhysRevResearch.4.033044

I. INTRODUCTION

The La-based high-T_c superconducting cuprate is a typical Mott system and has a rich variety in physics, making this system still mysterious and brightly fascinating even after three decades have passed since its discovery. There are open questions on exotic electronic states that need to be investigated, like pseudogaps [1], stripes of spins and holes [2], precursor of superconducting states [3], unconventional normal states [4], and charge-ordered states [5]. These unique states are commonly realized on the basis of the strong on-site Coulomb potential, U, and covalent states of Cu $3d$ orbitals with surrounding O $2p$ orbitals [6–14]. Both properties have been suggested to be essential to describe the possible mechanism of the high-T_c superconductivity because those carry the symmetry of the wave function of the Cooper pair and electronic conducting properties [15,16].

For deeper understanding of those exotic effects caused by the on-site Coulomb potential on Cu, U, and the covalent state, the mother system of the La-based high-T_c superconducting cuprate, La_2CuO_4 (LCO), can provide an ideal playground. LCO is a typical Mott insulator and has the strong covalent state of Cu $3d$ with O $2p$ within the two-dimensional CuO_2 plane. The antiferromagnetic (AF) interaction between Cu spins leads to the formation of the AF ordered state [17–20]. The exchange coupling energy within the CuO_2 plane was suggested to be about 140 meV

*Corresponding author: redo.ramadhan@idu.ac.id; Present address: Department of Chemical Engineering, Faculty of Industrial Technology, Universitas Pembangunan Nasional "Veteran" Yogyakarta, Sleman, Yogyakarta 55283, Indonesia.
†Present address: Department of Physics, Universitas Cokroaminoto Palopo, Kota Palopo 91911, Indonesia.
‡Present address: Innovative Global Program, College of Engineering, Shibaura Institute of Technology, Saitama 337-8570, Japan.
§Joint address: USM-RIKEN Interdisciplinary Collaboration for Advanced Sciences, School of Distance Education, Universiti Sains Malaysia, 11800 Minden, Pulau Pinang, Malaysia; Present address: Graduate School of Engineering and Science, Shibaura Institute of Technology, Saitama 337-8570, Japan.
‖Joint address: USM-RIKEN Interdisciplinary Collaboration for Advanced Sciences, School of Distance Education, Universiti Sains Malaysia, 11800 Minden, Pulau Pinang, Malaysia.
¶Corresponding author: budhy.kurniawan@sci.ui.ac.id.
#Present address: Department of Natural Sciences, Tokyo Denki University, Tokyo 120-8551, Japan.
**Corresponding author: nabedon@riken.jp

[21]. The value of U on the Cu atom has been well investigated but still has large ambiguities of 3–10 eV [6–14], giving uncertainty on discussions of exotic electronic states of high-T_c superconducting cuprates. This is because those features contain quantum and multibody effects of electrons which are still difficult to approach either experimentally or theoretically.

Following this situation, we suggest an approach to this problem by combining the muon spin rotation (μSR) measurement with the density functional theory (DFT) calculation including U as an adjustable parameter (DFT + U) [22–24]. The muon is a sensitive local magnetic probe and can trace the covalent state with the help of DFT + U. In this paper, we are going to show the results of this combined investigation on LCO, revealing the covalent state of Cu spins and determining U. We found three muon sites in LCO. Those muon positions were described from our DFT + U with the full view of the spatial distribution of Cu spins caused by the covalent state. Adjusting DFT + U with the μSR results, we obtained the U value to be 4.87(4) eV followed by the determination of the minimum charge-transfer (CT) energy between the upper Hubbard band of Cu $3d_{x^2-y^2}$ and O $2p$ to be 1.24(1) eV, and the size of the magnetic moment of Cu spin to be 0.520(3) μ_B.

II. EXPERIMENTALS

A. Growth of the La_2CuO_4 single crystal

A large LCO single crystal was synthesized by the traveling-solvent floating-zone method and was confirmed to be of a single phase without impurities by using x-ray-diffraction measurement at room temperature. After oxygen reduction annealing in Ar-gas flow, the AF transition temperature, T_N, was estimated from the magnetic susceptibility measurement by using a superconducting quantum interference device (Quantum Design Co. Ltd., MPMS-XL). The crystal was sliced in parallel with the CuO_2 layer for present μSR measurements.

B. μSR

μSR measurements were carried out on the GPS spectrometer at the Paul Scherrer Institut (PSI) in Switzerland by using a continuous muon source in the zero-field condition. The muon was injected into the LCO single-crystal sample keeping the initial spin polarization perpendicular to the CuO_2 plane. The time dependence of the asymmetry parameter, $A(t)$, is defined as $A(t) = \frac{F(t)-B(t)}{F(t)+B(t)}$ (μSR time spectrum). Here, $F(t)$ and $B(t)$ are numbers of positrons counted by the forward and backward counters at t, respectively [25,26]. In order to determine internal fields at muon sites with higher accuracy, we gathered more than 6×10^8 positrons which were more than 20 times higher than usual cases.

C. DFT calculations

DFT calculations were conducted using the Vienna *Ab-Initio* Simulation Package (VASP) [27,28] with the Generalized Gradient Approximation Perdew-Wang91 (GGA-PW91) exchange-correlation functional with adjusting U between 2 and 8 eV [23,29]. The Kohn-Sham approach using the projector augmented-waves formalism was adopted as implemented in VASP [27,28]. It should be noted that DFT results generally depend on the functional [30]. Although GGA+U is neither ideal nor the best functional to exactly describe the electronic state of LCO, this functional is well known to be valid with U in order to describe electronic states of strongly correlated systems [6,9]. Since there is no ideal full self-interaction correlated functional even now, we chose GGA+U as the "best possible" functional for the present paper as well as other published papers [24].

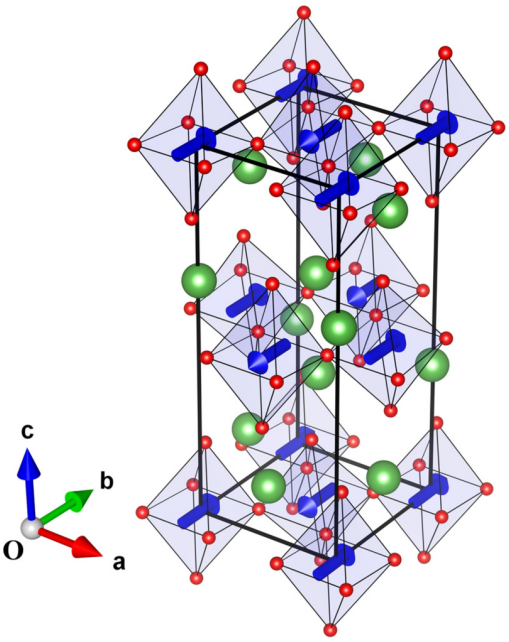

FIG. 1. Initial condition of the Cu-spin structure for the present DFT calculation study. Blue, red, and green marks are Cu spins, O, and La atoms, respectively. Cu spins form the AF spin alignment with the spin direction along to the b axis within the CuO_2 plane. This spin structure is the same as that determined from the neutron-scattering experiment [18].

The ground state of a calculation model was achieved by setting the convergence criterion of 1×10^{-4} eV. The relaxation process of all atomic positions was terminated until the magnitude of the force on each atom became less than 0.05 eV/Å following the quasi-Newton algorithm. The crystal structural symmetry was set to be orthorhombic with the *Bmab* space group. Lattice parameters for the unit cell were set to be $a = 5.3568$ Å, $b = 5.4058$ Å, and $c = 13.1432$ Å as estimated by the neutron-scattering experiment [31].

Figure 1 indicates an initial condition of the Cu-spin structure for present DFT calculations. Cu spins form the AF alignment with the spin direction in parallel with the b axis within the CuO_2 plane. This spin structure is the same as that determined from the neutron-scattering experiment [18]. The supercell containing 32 unit cells with one muon in the formation of the $4 \times 4 \times 2$ stacking was used for all our noncollinear DFT calculations to estimate stable muon positions. RIKEN Supercomputing Facility's HOKUSAI was used for our supercell calculations.

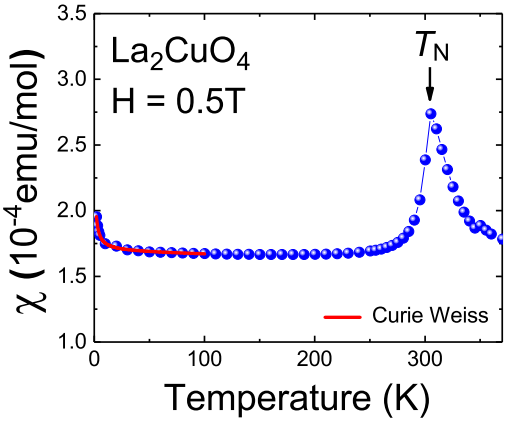

FIG. 2. Temperature dependence of the magnetic susceptibility of the La_2CuO_4 single crystal. The magnetic field of 0.5 T was applied perpendicular to the CuO_2 plane. The black arrow shows the antiferromagnetic transition temperature T_N of 309 K. The red solid line indicates the best-fit result by using the Curie-Weiss law below 100 K.

III. RESULTS

A. Characterizations of the La_2CuO_4 single crystal

Figure 2 shows the temperature dependence of the magnetic susceptibility of the LCO single crystal which was used for the present μSR study. The magnetic field of 0.5 T was applied perpendicular to the CuO_2 plane. A sharp peak was observed around 309 K which was due to the appearance of the long-range AF ordering of Cu spins [18,31]. An increase in the magnetic susceptibility was observed below about 20 K. This increase was fitted by the Curie-Weiss law. The red solid line in Fig. 2 is the best-fit result within the temperature range below 100 K. The Weiss temperature was estimated from this low-temperature analysis to be $-1.2(2)$ K. This result indicates that the increase in the magnetic susceptibility below 20 K is due to free spins which are not related to the AF ordering. Assuming that those free spins would be coming from Cu spins which appear around crystal defects, its fraction was estimated to be 0.024%.

B. μSR

Figure 3(a) shows the μSR time spectrum measured in the zero-field condition at 1.7 K on the LCO single crystal. The observation of the muon spin precession proved that Cu spins in LCO were in the AF ordered state [19]. The μSR time spectrum showed many turns of the muon spin with the slow damping rate. The muon spin precession was apparent at least up to 6 μs which was the reliable maximum measurable time. The observation of the clear muon spin recession in the long-time region indicates that the AF network of Cu spins is well coherent compared to those used in other μSR studies [19,20,32].

Figure 3(b) shows the Fourier spectrum of the muon spin precession. We confirmed three peaks. One was the main peak with a large spectral weight compared with the other two. The other two peaks were found at the higher- and lower-frequency sides with much smaller spectral weight than that of

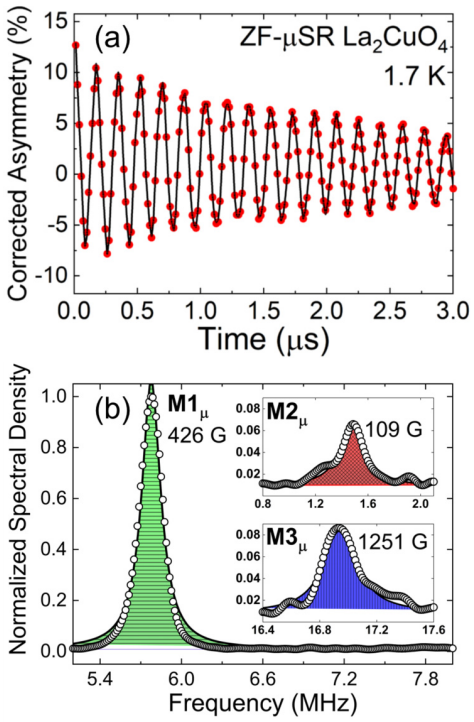

FIG. 3. (a) μSR time spectrum measured at 1.7 K on the La_2CuO_4 single crystal. The solid line is the best-fit results by using Eq. (1) with i=1,2,3. (b) Fourier spectrum of the muon spin precession. Solid lines show the best-fit results obtained by using the Lorentzian function. Insets show Fourier spectra of the additional two components.

the main peak. These results mean that there are three possible muon stopping positions in LCO with different occupancies. For convenience, we named the main peak, lower field, and higher field positions as $M1_\mu$, $M2_\mu$, and $M3_\mu$, respectively.

We applied the Lorentzian function to estimate the internal field at each muon site. Solid lines in Fig. 3(b) are the best-fit results for each peak. The frequency value at each peak position, ω, was converted to an internal magnetic field at the muon site, H, by the following relation:

$$\omega = \gamma_\mu H. \quad (1)$$

Here, γ_μ is the gyromagnetic ratio of μ of 135.5 MHz/T. The main peak is corresponding to the internal field of 426.7(1) G ($\approx$5.78 MHz). This value is the same as that reported in the past [19]. The low-frequency one is corresponding to 109.2(4) G ($\approx$1.48 MHz). This low-frequency peak was reported from the μSR study on the LCO thin film with much bigger muon-precession amplitude compared to our observed one in the bulk LCO single crystal [32]. At this moment, reasons why the amplitudes obtained in the LCO thin film and the bulk form are different are still unclear and need to be investigated. On the other hand, the high-frequency peak with the internal field of 1251.6(3) G ($\approx$17.0 MHz) was not reported in the LCO thin film. There is a possibility that this high-frequency peak was not clearly observed in the LCO thin film for some reason, such as too low precession amplitude.

TABLE I. Obtained parameters from the best fit of the μSR time spectrum by using Eq. (2) and Fourier spectra by using the Gaussian function. The ω_i was converted to the internal field at each muon site, $H^{\mathrm{Mi}}_{\mu\mathrm{SR}}$, following Eq. (1).

	μSR time spectrum				Fourier spectra
	A_i (%)	$H^{\mathrm{Mi}}_{\mu\mathrm{SR}}$ (G)	ϕ_i (deg)	λ_i (μs^{-1})	Peak position (G)
M1$_\mu$	9.228(23)	426.35(2)	−5.15(15)	0.333(20)	426.59 (1)
M2$_\mu$	2.631(54)	95.9(58)	22.6(55)	5.36(26)	109.16 (39)
M3$_\mu$	0.872(26)	1245.54(36)	−5.7(17)	0.50(3)	1251.55 (27)
Offset	1.879(54)	–	–	0.380(36)	–

Following this result, the time spectrum shown in Fig. 3(a) was analyzed assuming three muon sites by applying Eq. (2). Watching the time spectrum carefully, the center of the muon spin precession is shifted from the corrected zero-asymmetry position and relaxed slowly. The shift of the time spectrum from the corrected zero position was included in the analysis function as the offset component. Constant background signals which were coming from surroundings of the sample were subtracted from the time spectrum by applying this fitting method, so that the μSR time spectrum shown in Fig. 3(a) is the background-free spectrum. The solid line in Fig. 3(a) is the best-fit result:

$$A(t) = \sum_i A_i \cos(\omega_i t + \phi_i) e^{-\lambda_i t} + A_{\mathrm{offset}} e^{-\lambda_{\mathrm{offset}} t}. \quad (2)$$

Here, A_i and A_{offset}, and λ_i and $\lambda_{\mathrm{offset}}$, are initial asymmetries at t=0, relaxing rates of the muon spin precession and the offset component, respectively. The ω_i and ϕ_i are the frequency and phase of the muon spin precession, respectively. The ω_i is converted to the internal field at the muon site following Eq. (1). For convenience sake, we indexed the internal field at each muon site to be $H^{\mathrm{Mi}}_{\mu\mathrm{SR}}$ (i=1,2,3). The ratio among A_i is corresponding to the existing probability of the muon at each stopping site, putting i=1,2,3 for M1$_\mu$, M2$_\mu$, and M3$_\mu$, respectively. All parameters obtained from the Fourier analysis and direct fitting of the time spectrum are listed in Table I.

The ratio among initial asymmetries seems to be different from that of the Fourier spectrum weight. This is due to the fast relaxation rate for M2$_\mu$ compared to those for M1 and M3. After compensating the Fourier spectrum wight by the relaxation rate, both ratios became similar to each other. Accordingly, we used the ratio among initial asymmetries for simplicity to argue the population of the muon at each site.

C. DFT + U without μ

In the first attempt to combine DFT + U with the μSR results, we tried to visualize the full view of the covalent state of Cu around the the nuclear position without the muon. Figure 4(a) exhibits the map of the Cu-spin density distribution obtained from DFT + U calculations. The U was simply set to be 5.0 eV as a convenience. The Cu-spin density on the CuO_2 plane expands from the atomic position of Cu to the in-plane O sites. This is due to the covalent state of Cu $3d_{x^2-y^2}$ with the neighboring O $2p_\sigma$ and causes the appearance of a partial density of Cu spin at the in-plane O position. The adjacent Cu spin also expands its density to the same in-plane O site with the opposite sign of the spin direction and cancels the net magnetic moment at in-plane O. We found that about 18% of the Cu spin was transferred from the atomic position of Cu to in-plane O. This should be one of the reasons why the net magnetic moment of the Cu spin (S=1/2) is not 1 μ_B but reduced to be about a half as observed by neutron-scattering experiments [18,31]. This reduction due to the covalent state explained only 36% of the total reduction in the magnetic moment of Cu, indicating that the quantum spin fluctuation effect is important to satisfy the difference [33].

In addition to this, a small amount of the asymmetric Cu-spin density was found in $2p_z$ of apical O as indicated in Fig. 4(a). The estimated amount was at most 1% of the Cu spin, and the density inside the CuO_6 octahedron is bigger than that of the outside. This result is consistent with that obtained by Lane *et al.* [13]. Consequently, the net magnetic moment at apical O is not canceled and the amount of about 0.01 μ_B is left. The spin direction on apical O is opposite to that of Cu within the same CuO_6 octahedron. This small

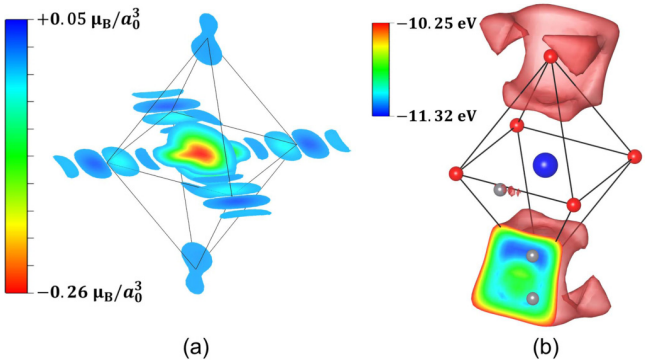

FIG. 4. (a) Three-dimensional map of the Cu-spin density in the CuO_6 octahedron of La_2CuO_4 obtained from our DFT + U calculations. The Cu-spin density expands to the in-plane O and reverses the spin direction at the other side centering the nuclear position of O as shown by the dark blue color. This means that the neighboring Cu-spin component which has the opposite spin direction as shown in Fig. 1 flows into the same in-plane O and cancels the total spin component. The a_0 in the density unit is the Bohr radius. (b) Electrostatic potential calculation results. The red area is the isosurface showing the energy level of 1.07 eV higher from the minimum potential. The energy level of the isosurface was chosen to make the position of M3$_{\mathrm{DFT}}$ clearly visible. Gray balls indicate three local-minimum potential positions as candidates for initial muon stopped positions.

magnetic moment at apical O cannot be ignored in the estimation of the internal field at the muon site [34].

The Cu-spin density in the vertical direction to the CuO_2 plane was also investigated by DFT in order to visualize a magnetic path along the interplane direction within the CuO_6 octahedron. However, almost no enlargement of the polarized spin-density distribution in Cu $3d_{z^2-r^2}$ was found in the preceding study [13], indicting a possibility that the interplane magnetic interaction could be driven by the direct exchange interaction between Cu $3d_{x^2-y^2}$ and $2p_z$ of apical O within the same CuO_6 octahedron. On the other hand, the angle-resolved photoelectron spectroscopy succeeded to visualize Cu $3d_{z^2-r^2}$ and a ^{139}La-NMR measurement pointed out a part of Cu-spin density was transferred to apical O via Cu $3d_{z^2-r^2}$ [35,36]. A theoretical study of low-energy Hamiltonians hypothesized active roles of Cu $3d_{z^2-r^2}$ hybridizing with O $2p_z$ [12]. These results indicate that the contribution of Cu $3d_{z^2-r^2}$ to the interplane magnetic interaction is not negligible and still an open question.

D. DFT + U with μ

As the next step, DFT + U was carried out including the muon to reproduce the μSR results. For this purpose, muon positions in LCO were investigated in advance. The precise determination of muon positions in LCO has not yet been successful in the past and was left as a long-term fundamental problem in the muon community [32,37–41].

Figure 4(b) shows our estimation of initial stopping positions of injected muons in LCO obtained from simple electrostatic potential calculations by using a unit cell since the muon has a positive charge and prefers to sit down at the minimum electrostatic potential just after it stops in the sample [40]. Three possible local minimum potential positions were found as candidates of initial muon stopping positions. We named those three positions as $M1_{DFT}$, $M2_{DFT}$, and $M3_{DFT}$ in order to compare with the μSR results. The injected muon chooses one of those three positions to initially stop and moves to a local stable position interacting with surrounding atoms and electrons, causing local deformations of the crystal structure and electronic states in the vicinity of the muon [41,42]. There are four crystallographic equivalent sites of each muon position within the unit cell. We confirmed by using the present calculation condition including the muon that those sites were also magnetically equivalent within the calculation accuracy.

Since the number of injected muons is almost negligible compared with the number of atoms in the sample, the muon can be regarded as a superdilute magnetic impurity in DFT + U. This situation requires us to set a sufficiently large supercell structure with one muon inside in order to follow the realistic μSR experimental condition. Accordingly, the $4 \times 4 \times 2$ supercell was used for the present DFT + U including the muon. DFT calculation on a small cell with one muon is unrealistic because the number of muons is comparable to the number of unit cells of the sample in smaller cells [43]. Our modeled supercell contained 896 atoms and one muon. All atomic positions and electronic density distributions needed to be adjustable parameters within the supercell with only one muon as the magnetic impurity. This kind of supercell calculation requires larger-scale computation volume. We carried out this large-scale calculation by using the high-performance supercomputing cluster system of HOKUSAI in RIKEN.

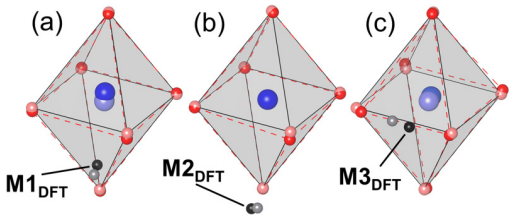

FIG. 5. Final stable muon positions for (a) $M1_{DFT}$, (b) $M2_{DFT}$, and (c) $M3_{DFT}$, respectively, obtained from DFT + U including the muon using the $4 \times 4 \times 2$ supercell. Gray and black balls in each panel indicate the initial and final position of the muon after the relaxation, respectively.

Figures 5(a)–5(c) indicate the final muon positions and local deformations of the crystal structure estimated from our DFT + U + μ calculations. As for $M1_{DFT}$, the muon is located near apical O and inside the CuO_6 octahedron as demonstrated in Fig. 5(a). The muon moves further inside of the CuO_6 octahedron after relaxing its position and pushes away the Cu atom from the muon. Two in-plane O in the CuO_2 plane are pulled toward $M1_{DFT}$. Concerning $M2_{DFT}$, the muon stops near apical O as well as $M1_{DFT}$ but outside the CuO_6 octahedron as shown in Fig. 5(b). The muon moves away a little from apical O after the relaxation and pulls one in-plane O to its side. $M2_{DFT}$ does not affect the Cu position too much. In terms of $M3_{DFT}$, the muon sits in between two in-plane O and pulls them to its side and pushes away the Cu atom from the muon as exhibited in Fig. 5(c).

Those local changes in atomic positions of Cu lead to changes in the Cu-spin distribution around the muon. Figure 6 shows the results of DFT + U + μ, indicating the Cu-spin density distribution around each muon position. In the case of $M1_{DFT}$, the Cu-spin density becomes slightly less as shown in Fig. 6(a), resulting in the reduction of the magnetic moment of Cu overall. This reduction in the magnetic moment of Cu happens just beside the muon. The reduction ratio of the magnetic moment of Cu in the presence of the muon was

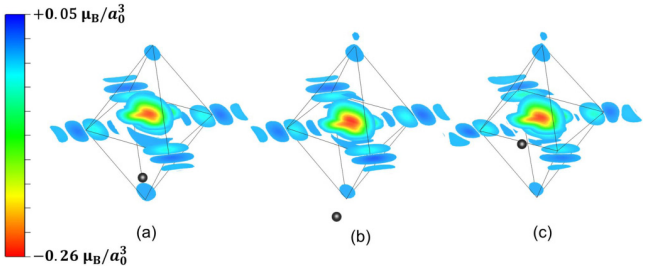

FIG. 6. Cu-spin density distribution estimated by DFT + U including the muon using the $4 \times 4 \times 2$ supercell with the muon at (a) $M1_{DFT}$, (b) $M2_{DFT}$, and (c) $M3_{DFT}$, respectively. Black balls in each panel indicate the final position of the muon after the relaxation where the muon's density has the maximum. The a_0 in the density unit is the Bohr radius.

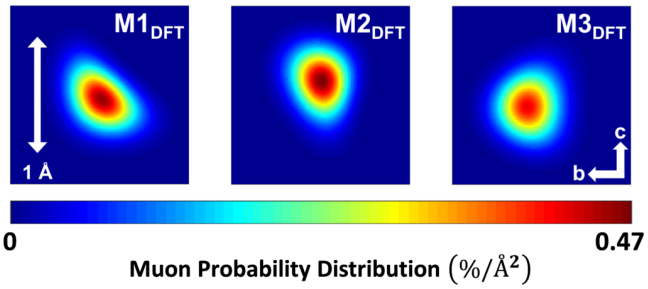

FIG. 7. Zero-point vibration motion of the muon itself around the minimum electrostatic potential for $M1_{DFT}$, $M2_{DFT}$, and $M3_{DFT}$. These are views of cross sections perpendicular to the CuO_2 plane including the local minimum potential point.

estimated to be about -5 and -1% for $M1_{DFT}$ and $M3_{DFT}$, and $\approx 0\%$ for $M2_{DFT}$.

The unbalanced spin density was also found at in-plane O which was caused by changes in the spin densities coming from the adjacent two Cu atoms. This effect was the largest for $M3_{DFT}$ as shown in Fig. 6(c) and can be qualitatively understood as follows. The balance of the Cu-spin density transferred to in-plane O is broken due to deformations of local electronic states and crystal structure which happens at one side beside the muon. This unbalanced Cu-spin density at in-plane O causes the nonzero magnetic moment. The estimated size of the additional magnetic moment was about 0.01 μ_B but cannot be negligible for the estimation of the internal field at the muon site because this component appears just near the muon. Similarly, the small component of the magnetic moment at apical O slightly increased due to the change in the local Cu-spin density. All of these changes are local effects induced by the injected muon and disappear quickly beyond next neighbor unit cells.

E. Effects of the zero-point vibration motion of μ

In preceding studies, internal fields at the muon sites were always overestimated and could not explain the present μSR results even taking into account distributed Cu spins as shown in Figs. 6(a)–6(c). Accordingly, we included one quantum effect of the muon itself, which was the zero-point vibration motion [44]. This is because the muon is a fine particle with the lighter mass of about 1/9 compared to the hydrogen and has the spatial distribution around the stopping position following the shape of the local potential. This quantum motion of the muon can be obtained by solving the Schrödinger equation around the local potential surrounding the muon as follows:

$$\left[-\frac{\hbar^2\nabla^2}{2m_\mu} + V_\mu(r)\right]\psi_\mu(r) = E_\mu\psi_\mu(r). \tag{3}$$

Here, $V_\mu(r)$, m_μ, $\psi_\mu(r)$, and E_μ are the potential around the muon, muon's mass, wave function, and eigenvalue, respectively. The Schrödinger equation was solved numerically by using the MATLAB program.

Figure 7 shows the estimated muon spin distribution due to the zero-point vibration motion around the minimum electrostatic potential for $M1_{DFT}$, $M2_{DFT}$, and $M3_{DFT}$. These are two-dimensional images within the cross section along the CuO_2 plane. Red- and blue-color regions indicate the high and low muon-density areas, respectively. We confirmed that more than 99% muon density is there within the 1.5-Å^3 cubic volume. The total sum of the dipole fields from surrounding Cu spins is calculated taking into account this muon spin density distribution.

IV. DISCUSSIONS

In order to optimize muon positions and other related parameters, the internal fields at $M1_{DFT}$, $M2_{DFT}$, and $M3_{DFT}$ were calculated on the basis of the dipole-dipole coupling, because LCO is a good insulator and the existing probability of conducting electrons around the muon is expected to be unlikely [45]. Cu-spin distributions and the muon's zero-point vibration motion were also included in the estimation of the internal field by using the following equation:

$$\sum_{i,j}\frac{1}{|\vec{r}_i-\vec{r}_j|^3}\left[3\vec{\rho}_i(\vec{r}_i-\vec{r}_j)\frac{(\vec{r}_i-\vec{r}_j)}{|\vec{r}_i-\vec{r}_j|^2}-\vec{\rho}_i\right]|\psi_j|^2. \tag{4}$$

Here, $\vec{\rho}_i$ denotes the vector data for the spin grids and $\vec{r}_i - \vec{r}_j$ denotes the relative distance between the Cu-spin-density grids with the density of ρ_i and the muon probability grids $|\psi_j|^2$. Then, we summed up all grid components obtained from our DFT calculations to estimate the internal field at the muon site. We set the radius of 50 Å centering the muon to achieve the converged results for dipole calculations. The supercell with one muon was set at the center of the calculated sphere and other areas were filled up by normal unit cells without muons.

It should be noted that multiple magnetic sites can be realized when different spin-structure domains are induced around microscopic defects in the LCO crystal as suggested from the μSR study on the LCO thin film [32]. If this is the case, those defects are expected to introduce free Cu spins as well around defects in the Cu-spin network [46,47]. Our magnetic susceptibility measurement on the LCO single crystal showed that the fraction of those kinds of free spins is very small and almost negligible. This result means that the LCO single crystal used in the present paper has less defects, indicating the uniform Cu-spin network with a single spin-structure domain.

We have already simulated internal fields at three muon sites in LCO with some different spin structures including the ones suggested from the μSR study on the LCO thin film [48]. This previous result showed that three different internal fields at our estimated three muon sites in the LCO single crystal can be quantitatively explained by one magnetic domain even though different spin states were set. Accordingly, we assumed in the present paper that one uniform magnetic spin structure which was the same as that determined from the neutron-scattering experiment appeared in the LCO single crystal [17,18], and thus the existence of three muon sites in LCO was intrinsic.

Since all muon positions, magnetic moments of Cu, and Cu-spin density distributions are related to U, the dipole-field calculation was repeated varying U from 2 to 8 eV in order to

TABLE II. Top part: Magnetic moment of the Cu spin estimated from current DFT calculations without the muon by varying U. Bottom part: Calculated internal fields at $M1_{DFT}$, $M2_{DFT}$, and $M3_{DFT}$ obtained from DFT calculations by varying U. All calculations were done with the same conditions taking into account the local deformation of the crystal structure and electronic state lead by the muon. The zero-point vibration motion of the muon was also included in the calculation.

	U (eV)												
	2	3	3.5	4	4.5	5	5.6	6	6.5	7	7.2	7.5	8
	Calculated magnetic moment without μ (μ_B)												
Magnetic moment	0.386	0.436	0.460	0.482	0.503	0.524	0.547	0.562	0.583	0.602	0.609	0.621	0.641
Muon position	Calculated internal fields, H^{Mi}_{DFT} (G)												
$M1_{DFT}$	336.35	376.01	384.85	391.51	429.28	446.36	450.22	471.50	474.90	491.08	503.83	507.16	523.10
$M2_{DFT}$	103.99	116.30	121.28	127.04	131.21	135.68	141.54	145.85	150.14	154.33	155.44	159.07	163.76
$M3_{DFT}$	888.06	990.60	1038.67	1077.89	1128.28	1169.74	1219.72	1241.02	1281.64	1322.98	1334.41	1364.36	1407.01

find out the optimized results. All calculated values which we have done are summarized in Table II.

Based on those results, we indexed the calculated internal fields as H^{Mi}_{DFT} (i=1,2,3) in order to compare with $H^{Mi}_{\mu SR}$. And then, we defined differences between both values by using the following equation:

$$\Delta H_{Mi} = \left(H^{Mi}_{DFT} - H^{Mi}_{\mu SR}\right), \quad (i = 1, 2, 3). \tag{5}$$

After this, we summed up all ΔH_{Mi} for each U with fitting-error values of internal fields, σ_i, as follows (detailed values of σ_i are listed in Table I):

$$\sum_i \frac{\Delta H^2_{Mi}}{\sigma_i^2}, \quad (i = 1, 2, 3). \tag{6}$$

Figure 8 shows the U dependence of summed up values obtained from Eq. (6). Applying the Gaussian function, U was optimized to be 4.87(4) eV. This value locates at the lower end of the U range which has been argued to be from 3 to 10 eV [6–14].

It was pointed out from theoretical studies on the Hubbard model with a square lattice that U is strongly correlated to the energy scale of the effective spin Hamiltonian which is described as $4t^2/U$ and that a border between strong and weak

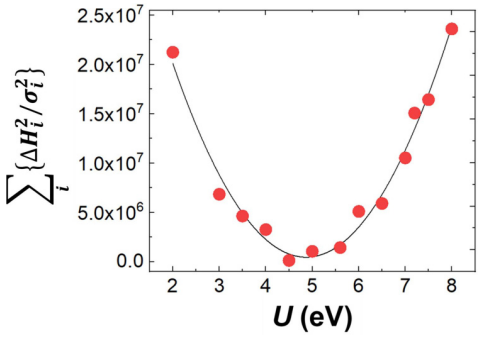

FIG. 8. Optimization of U in terms of the difference in internal fields obtained by μSR and DFT + U + μ calculations, varying U from 2 to 8 eV. The solid line is the best-fit result by using the Gaussian function. ΔH_{Mi} is the difference between $H^{Mi}_{\mu SR}$ and H^{Mi}_{DFT} (i=1,2,3) as described in Eq. (5). σ_i is the fitting-error value of the internal field at each $H^{Mi}_{\mu SR}$.

correlations is around $U \approx 6.5t$ [16]. Here, t is the hopping energy of electrons. Our present result of the smaller U in LCO would give limitations on discussions of t and provide possible dedicated directions to understand differences in T_c among high-T_c superconducting cuprates [49]. For instance, we suggest following the *Ab-Initio* calculation of the effective Hamiltonian that the electronic state of LCO is closer to the one-band model although more detailed comparisons with theoretical investigations are necessary [12].

Following this result of the optimization of U, the magnetic moment of Cu was estimated through the same DFT calculation processes. The optimized value was 0.520(3) μ_B in the case of LCO without the muon. The direction of the optimized Cu spin was still along the b-axis after the noncollinear refinement. The estimated magnetic moment and the spin structure were consistent with those suggested from neutron-scattering experiment [18]. In addition, optimized internal fields at each muon site in the case of U = 4.87(4) eV were calculated from the dipole-field calculation using Eq. (4) to be 429.7(12), 134.1(4), and 1,147.6(35) G for $M1_{DFT}$, $M2_{DFT}$, and $M3_{DFT}$, and thus $M1_{DFT} = M1_\mu$, $M2_{DFT} = M2_\mu$, and $M3_{DFT} = M3_\mu$, respectively. Differences in the internal field between the μSR and DFT + U + μ were 3.4 (≈1%), 38.2 (≈ 40%), and 97.9 G (≈ 8%) for $M1_\mu$, $M2_\mu$, and $M3_\mu$, respectively. All optimized muon positions and internal fields are summarized in Table III. Atomic positions of the CuO_6 octahedron after the optimization with the muon at $M1_{DFT}$, $M2_{DFT}$, and $M3_{DFT}$ are listed in Table IV.

Figure 9 indicates the simulated μSR time spectrum by using internal fields obtained from present DFT + U + μ calculations. We used the same values for A_i, ϕ_i, and λ_i as listed in Table I and H^{Mi}_{DFT} in order to evaluate our DFT results. The solid-red line in Fig. 9 is the simulation result. The simulated result reproduced the time spectrum fairly well, but there were still small differences between measured and simulated μSR time spectra, especially in the longer time region. This is because simulated internal fields for M1 and M3 are very close to the experimental results but the one for M2 is still fairly far. The reason why our DFT + U + μ did not perfectly reproduce the experimental result is guessed to be due to DFT's underlying principal statistical errors with regards to the pseudopotential approximation, calculation-grid resolution, cutoff energy, relaxation step for self-consistent calculation loop,

TABLE III. Cartesian components of optimized muon positions in the 4 × 4 × 2 supercell and internal fields at each muon position in the style of the normalized component against the unit-cell size along the *a*-, *b*-, and *c*-axis. The definition of each crystal axis was the same as that used in the neutron-scattering experiment [18]. The negative signature means that internal fields direct opposite.

	Before relaxation			After relaxation			Internal fields (G)				
Muon position	*a*	*b*	*c*	*a*	*b*	*c*	Fourier	DFT	*a*	*b*	*c*
$M1_{DFT}$	0.3839	0.5982	0.4336	0.3777	0.6175	0.4375	426.59(1)	429.7(12)	−2.81	355.06	−241.92
$M2_{DFT}$	0.3928	0.5893	0.4023	0.3817	0.5968	0.3975	109.16(39)	134.1(4)	−8.54	73.89	−111.04
$M3_{DFT}$	0.3660	0.5491	0.4961	0.3880	0.5502	0.4935	1251.55(27)	1147.6(35)	23.47	−1134.59	−170.17

and so on. Although the DFT + U calculation has been well established to describe electronic states of strongly correlated systems [6–14,24,42] and those statistical errors should be small, errors would be piled up during the total-energy minimization process of the nonperiodical supercell model with the muon and become nonignorable as a result in our case.

It is worthwhile to describe other value-added results obtained from the present DFT study. By using the optimized U, the band-gap structure can also be optimized, leading to the minimum CT gap between the upper Hubbard band and O 2*p* being 1.24(1) eV. This CT-gap value has been discussed within the range of 0.9–2 eV giving large ambiguity [13,50–52]. Note that our obtained value is in the ground state at 0 K. Even taking into account that the measured CT gap shows a shift for a couple of 0.1 eV to the lower-energy side with increasing temperature [52], our obtained value is fully consistent with the previous results [13,50–52]. Those facts also proved that our results revealed the realistic feature of the electronic state of LCO.

There is still one more question left for the full understanding of the μSR results. That is how to explain differences in populations of stopped muons among the three sites. The experimental results indicate that most of the injected muons stop at $M1_{\mu}$ as evidenced in Fig. 3(b). The ratio of populations of muons among those three sites was determined from the differences in the initial asymmetries to be $M1_{\mu}$:$M2_{\mu}$:$M3_{\mu}$=106:30:10. One possible way to address this question is to model the stopping procedure of the muon in LCO after its injection. This is left as an open question. More DFT calculations and/or simulations will be required to tackle this problem.

V. CONCLUSION

We determined the value of U, the covalent state of the Cu spin, and the CT gap energy in LCO by combining μSR experiments and DFT calculations. Three muon positions in LCO were identified and U was precisely determined to be 4.87(4) eV, the magnetic moment of Cu was determined to be 0.520(3) μ_B, and the minimum CT gap between the upper Hubbard band and the O 2*p* band was determined to be 1.24(1) eV. The role of the perturbation introduced by the muon was found to deform the local crystal structure just around the muon, followed by subsequent changes in the surrounding electronic state in LCO. This effect leads to the slight reduction in the magnetic moment surrounding the muon.

A strong benefit of our technique is that we can achieve information of the spin structure, size of the magnetic moment, muon positions, and U in one time by analyzing one μSR time spectrum. Especially, the U value cannot be optimized from other experimental methods with good accuracy as demonstrated in the present paper. In addition, our technique is workable for other systems on the basis of some experimental and computational conditions.

(1) The target system has magnetic moments.
(2) The muon spin precession should be observed.
(3) DFT calculation is applicable.
(4) There are accessible high-performance computing resources which can accept large-scale supercell calculations.

TABLE IV. Cartesian components of atomic positions in the 4 × 4 × 2 supercell before and after the optimization of the CuO_6 octahedron with the injected muon at $M1_{DFT}$, $M2_{DFT}$, and $M3_{DFT}$, respectively. Each atomic position in the CuO_6 octahedron is indicated in the figure at the right end of the table. All positions are described in the style of the normalized component against the unit-cell size along the *a*-, *b*-, and *c*-axis. The definition of each crystal axis was the same as that used in the neutron-scattering experiment [18].

	before relaxation			after relaxation								
	without μ			with μ at $M1_{DFT}$			with μ at $M2_{DFT}$			with μ at $M3_{DFT}$		
Atoms	*a*	*b*	*c*	*a*	*b*	*c*	*a*	*b*	*c*	*a*	*b*	*c*
Cu	0.3750	0.6250	0.5000	0.3751	0.6243	0.5087	0.3757	0.6240	0.5003	0.3739	0.6322	0.5024
O_1	0.3125	0.5625	0.4964	0.3128	0.5635	0.4915	0.3125	0.5620	0.4942	0.3202	0.5597	0.4932
O_2	0.4375	0.5625	0.4964	0.4369	0.5639	0.4891	0.4377	0.5622	0.4874	0.4350	0.5623	0.4929
O_3	0.4375	0.6875	0.5036	0.4373	0.6876	0.5056	0.4381	0.6869	0.5042	0.4376	0.6898	0.5084
O_4	0.3125	0.6875	0.5036	0.3128	0.6876	0.5059	0.3133	0.6872	0.5043	0.3102	0.6891	0.5087
O_5	0.3750	0.6165	0.5918	0.3755	0.6112	0.5917	0.3766	0.6122	0.5918	0.3762	0.6079	0.5927
O_6	0.3750	0.6335	0.4018	0.3742	0.6402	0.4052	0.3733	0.6408	0.4057	0.3753	0.6418	0.4076

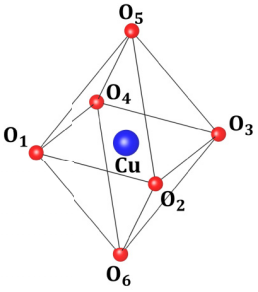

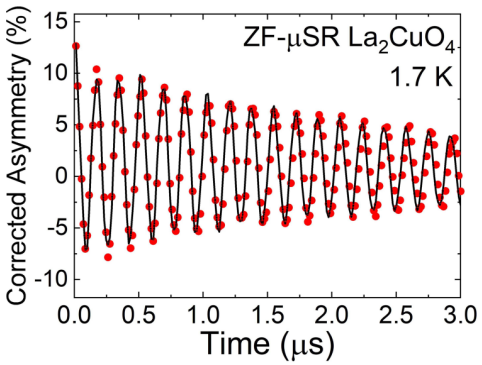

FIG. 9. ZF-μSR time spectrum observed at 1.7 K with the simulated line by using internal fields which were estimated from the current DFT calculations. The black solid line is the trace of the simulation. The same values for A_i, ϕ_i, and λ_i listed in Table I were used, replacing $H^{Mi}_{\mu SR}$ with H^{Mi}_{DFT} to draw the black solid line.

As long as those four conditions are satisfied, our developed technique to estimate U is widely applicable to any systems. For instance, mother systems of all Cu-based high-T_c cuprates, Mott systems, heavy fermions, and strongly correlated organic molecular systems are good targets. Even using other DFT package programs like QUANTUM ESPRESSO, CASTEP, and WIEN2K, one can apply the same method described in this paper to one's own target materials. This means that the transferability of our method to other materials is quite high and widely applicable to other research fields, providing us deeper knowledge on their unique and exotic properties from a different perspective via μSR.

ACKNOWLEDGMENTS

The authors would like to thank for technical support the muon group of PSI for carrying out the μSR measurement and they also thank K. Ishida, A. Fujimori, and M. Ogata for valuable discussions. We would like to acknowledge the HOKUSAI supercomputing facility (Project No. G19007) of RIKEN. This work is supported by Japan Society for the Promotion of Science KAKENHI (Grants No. JP19H01841 and No. 20H04463) and International Program Associate of RIKEN.

[1] T. Timusk and B. Statt, The the pseudogap in high-temperature superconductors: An experimental survey, Rep. Prog. Phys. **62**, 61 (1999).

[2] J. M. Tranquada, B. J. Sternlieb, J. D. Axe, Y. Nakamura, and S. Uchida, Evidence for stripe correlations of spins and holes in copper oxide superconductors, Nature (London) **375**, 561 (1995).

[3] Y. Wang, L. Li, and N. P. Ong, Nernst effect in high-T_c superconductors, Phys. Rev. B **73**, 024510 (2006).

[4] G. S. Boebinger, Y. Ando, A. Passner, T. Kimura, M. Okuya, J. Shimoyama, K. Kishio, K. Tamasaku, N. Ichikawa, and S. Uchida, Insulator-To-Metal Crossover in the Normal State of $La_{2-x}Sr_xCuO_4$ Near Optimum Doping, Phys. Rev. Lett. **77**, 5417 (1996).

[5] J. Chang, E. Blackburn, A. T. Holmes, N. B. Christensen, J. Larsend, J. Mesot, D. A. Ruixing Liang, Bonn, W. N. Hardy, A. Watenphul, M. V. Zimmermann, E. M. Forgan, and S. M. Hayden, Direct observation of competition between superconductivity and charge density wave order in $YBa_2Cu_3O_{6.67}$, Nat. Phys. **8**, 871 (2012).

[6] M. T. Czyżyk and G. A. Sawatzky, Local-density functional and on-site correlations: The electronic structure of $La_{2-x}Sr_xCuO_4$ and $LaCuO_3$, Phys. Rev. B **49**, 14211 (1994).

[7] V. I. Anisimov, M. A. Korotin, I. A. Nekrasov, Z. V. Pchelkina, and S. Sorella, First principles electronic model for high-temperature superconductivity, Phys. Rev. B **66**, 100502(R) (2002).

[8] X. Wan, T. A. Maier, and S. Y. Savrasov, Calculated magnetic exchange interactions in high-temperature superconductors, Phys. Rev. B **79**, 155114 (2009).

[9] S. Pesant and M. Côté, DFT + U study of magnetic order in doped $La_{2-x}Sr_xCuO_4$ crystals, Phys. Rev. B **84**, 085104 (2011).

[10] P. Werner, R. Sakuma, F. Nilsson, and F. Aryasetiawan, Dynamical screening in $La_{2-x}Sr_xCuO_4$, Phys. Rev. B **91**, 125142 (2015).

[11] S. W. Jang, A. Hirofumi, H. Kino, T. Kotani, K. Kuroki, and M. J. Han, Direct theoretical evidence for weaker correlations in electron-doped and Hg-based hole-doped cuprates, Sci. Rep. **6**, 33397 (2016).

[12] M. Hirayama, Y. Yamaji, T. Misawa, and M. Imada, Ab initio effective Hamiltonians for cuprate superconductors, Phys. Rev. B **98**, 134501 (2018).

[13] C. Lane, J. W. Furness, I. G. Buda, Y. Zhang, R. S. Markiewicz, B. Barbiellini, J. Sun, and A. Bansil, Antiferromagnetic ground state of La_2CuO_4: A parameter-free *ab initio* description, Phys. Rev. B **98**, 125140 (2018).

[14] F. Nilsson, K. Karlsson, and F. Aryasetiawan, Dynamically screened Coulomb interaction in the parent compounds of hole-doped cuprates: Trends and exceptions, Phys. Rev. B **99**, 075135 (2019).

[15] F. C. Zhang and T. M. Rice, Effective Hamiltonian for superconducting Cu oxides, Phys. Rev. B **37**, 3759(R) (1988).

[16] M. Yokoyama, H. Ogata and Y. Tanaka, Mott transitions and d-wave superconductivity in half-filled-band Hubbard model on square lattice with geometric frustration, J. Phys. Soc. Jpn. **75**, 114706 (2006).

[17] J. I. Budnick, A. Golnik, C. Niedermayer, E. Recknagel, M. Rossmanith, A. Weidinger, B. Chamberland, M. Filopkowski, and D. P. Yang, Observation of magnetic ordering in $La_{2-x}Sr_xCuO_4$ by muon spin spectroscopy, Phys. Lett. A **124**, 103 (1987).

[18] D. Vaknin, S. K. Sinha, D. E. Moncton, D. C. Johnston, J. M. Newsam, C. R. Safinya, and H. E. King, Antiferromagnetism in La_2CuO_{4-y}, Phys. Rev. Lett. **58**, 2802 (1987).

[19] Y. J. Uemura, Muon spin relaxation studies on T_c superconductors and related antiferromagnet, J. Appl. Phys. **64**, 6087 (1988).

[20] F. Borsa, P. Carretta, J. H. Cho, F. C. Chou, Q. Hu, D. C. Johnston, A. Lascialfari, D. R. Torgeson, R. J. Gooding, N. M. Salem, and K. J. E. Vos, Staggered magnetization in $La_{2-x}Sr_xCuO_4$ from ^{139}La-NQR and μ: Effects of Sr doping in the range $0 \leqslant x \leqslant 0.02$, Phys. Rev. B **52**, 7334 (1995).

[21] R. Coldea, S. M. Hayden, G. Aeppli, T. G. Perring, C. D. Frost, T. E. Mason, S.-W. Cheong, and Z. Fisk, Spin Waves and

Electronic Interactions in La_2CuO_4, Phys. Rev. Lett. **86**, 5377 (2001).

[22] V. I. Anisimov, J. Zaanen, and O. K. Andersen, Band theory and Mott insulators: Hubbard U instead of stoner I, Phys. Rev. B **44**, 943 (1991).

[23] S. L. Dudarev, G. A. Botton, S. Y. Savrasov, C. J. Humphreys, and A. P. Sutton, Electron-energy-loss spectra and the structural stability of nickel oxide: An LSDA + U study, Phys. Rev. B **57**, 1505 (1998).

[24] J. Varignon, M. Bibes, and A. Zunger, Origin of band gaps in 3*d* perovskite oxides, Nat. Commun. **10**, 1658 (2019).

[25] R. S. Hayano, Y. J. Uemura, J. Imazato, N. Nishida, T. Yamazaki, and R. Kubo, Zero-and low-field spin relaxation studied by positive muons, Phys. Rev. B **20**, 850 (1979).

[26] Y. J. Uemura, T. Yamazaki, D. R. Harshman, M. Senba, and E. J. Ansaldo, Muon-spin relaxation in AuFe and CuMn spin glasses, Phys. Rev. B **31**, 546 (1985).

[27] G. Kresse and J. Furthmöller, Efficiency of ab-initio total energy calculations for metals and semiconductors using a plane-wave basis set, Comput. Mater. Sci. **6**, 15 (1996).

[28] G. Kresse and J. Furthmüller, Efficient iterative schemes for *ab-initio* total-energy calculations using a plane-wave basis set, Phys. Rev. B **54**, 11169 (1996).

[29] J. P. Perdew, J. A. Chevary, S. H. Vosko, K. A. Jackson, M. R. Pederson, D. J. Singh, and C. Fiolhais, Atoms, molecules, solids, and surfaces: Applications of the generalized gradient approximation for exchange and correlation, Phys. Rev. B **46**, 6671 (1992).

[30] J. Kulik and N. Marzari, A self-consistentHubbard U density-functional theory approach to the addition-elimination reactions of hydrocarbons on bare FeO^+, Chem. Phys. **129**, 134314 (2008).

[31] M. Reehuis, C. Ulrich, K. Prokeš, A. Gozar, G. Blumberg, S. Komiya, Y. Ando, P. Pattison, and B. Keimer, Crystal structure and high-field magnetism of La_2CuO_4, Phys. Rev. B **73**, 144513 (2006).

[32] E. Stilp, A. Suter, T. Prokscha, E. Morenzoni, H. Keller, B. M. Wojek, H. Luetkens, A. Gozar, G. Logvenov, and I. Božović, Magnetic phase diagram of low-doped $La_{2-x}Sr_xCuO_4$ thin films studied by low-energy muon-spin rotation, Phys. Rev. B **88**, 064419 (2013).

[33] K. M. Kojima, Y. Fudamoto, M. Larkin, G. M. Luke, J. Merrin, B. Nachumi, Y. J. Uemura, N. Motoyama, H. Eisaki, S. Uchida, K. Yamada, Y. Endoh, S. Hosoya, B. J. Sternlieb, and G. Shirane, Reduction of Ordered Moment and Néel Temperature of Quasi-One-Dimensional Antiferromagnets Sr_2CuO_3 and Ca_2CuO_3, Phys. Rev. Lett. **78**, 1787 (1997).

[34] M. Miyazaki, R. Kadono, K. H. Satoh, M. Hiraishi, S. Takeshita, A. Koda, A. Yamamoto, and H. Takagi, Magnetic ground state of pyrochlore oxides close to metal-insulator boundary probed by muon spin rotation, Phys. Rev. B **82**, 094413 (2010).

[35] C. E. Matt, D. Suter, and J. Chang, Direct observation of orbital hybridization in a cuprate superconductor, Nat. Commun. **9**, 972 (2018).

[36] I. Watanabe, ^{139}La-NQR study of the magnetic properties of $La_{2-x}M_xCuO_4$(M = Ba, Sr) for $0 \leqslant x \leqslant 0.08$, J. Phys. Soc. Jpn. **63**, 1560 (1994).

[37] B. Hitti, P. Birrer, K. Fischer, F. N. Gygax, E. Lippelt, H. Maletta, A. Schenk, and M. Weber, Study of La_2CuO_4 and related compounds by μSR, Hyperfine Interact. **63**, 287 (1991).

[38] E. Torikai, K. Nagamine, H. Kitazawa, I. Tanaka, S. B. Kojima, Sulaiman, S. Srinivas, and T. P. Das, Behavior of positive muons in high T_c superconductors $La_{2-x}Sr_xCuO_4$, Hyperfine Interact. **79**, 921 (1993).

[39] S. B. Sulaiman, N. Sahoo, S. Srinivas, F. Hagelberg, T. P. Das, E. Torikai, and K. Nagamine, Theory of location and associated hyperfine properties of the positive muon in La_2CuO_4, Hyperfine Interact. **84**, 87 (1994).

[40] B. Adiperdana, I. A. Dharmawan, S. E. Siregar, I. Watanabe, K. Ohishi, Y. Ishii, T. Suzuki, T. Kawamata, R. Scheuemann, K. Sedlak, Y. Tomioka, T. Waki, Y. Tabata, and H. Nakamura, Muon sites estimation in La_2CuO_4 and a new vanadium cluster compound, $V_4S_9Br_4$, using electronic and nuclear dipole field calculations, Phys. Procedia **30**, 109 (2012).

[41] H. U. Suter, E. P. Sroll, and P. F. Meier, Muon sites and hyperfine fields in La_2CuO_4, Phys. B: Condens. Matter **326**, 329 (2003).

[42] J. S. Möller, P. Bonfà, D. Ceresoli, S. J. Bernardini, F. Blundell, T. Lancaster, R. De Renzi, N. Marzari, I. Watanabe, and S. B. Sulaiman, Playing quantum hide-and-seek with the muon: Localizing muon stopping sites, Phys. Scr. **88**, 068510 (2013).

[43] M. R. Ramadhan, I. Ramli, M. D. Umar, S. Winarsih, D. P. Sari, A. Manaf, B. Kurniawan, M. I. Mohamed-Ibrahim, S. Sulaiman, and I. Watanabe, Effect of the supercell's size on muon positions calculations of La_2CuO_4, Mater. Sci. Forum **966**, 465 (2019).

[44] F. Bernardini, P. Bonfà, S. Massidda, and R. De Renzi, Ab initio strategy for muon site assignment in wide band gap fluorides, Phys. Rev. B **87**, 115148 (2013).

[45] The contact field at the muon position estimated by VASP was less than 1 G indicating that the Cu-spin density at the muon position is nearly negligible.

[46] K. Kojima, A. Keren, G. M. Luke, B. Nachumi, W. D. Wu, Y. J. Uemura, M. Azuma, and M. Takano, Magnetic Behavior of the 2-Leg and 3-Leg Spin Ladder Cuprates $Sr_{n-1}Cu_{n+1}O_{2n}$, Phys. Rev. Lett. **74**, 2812 (1995).

[47] T. Adachi, N. Oki, Risdiana, S. Yairi, Y. Koike, and I. Watanabe, Effects of Zn and Ni substitution on the Cu spin dynamics and superconductivity in $La_{2-x}Sr_xCu_{1-y}(Zn, Ni)_yO_4x$=0.15-0.20): Muon spin relaxation and magnetic susceptibility study, Phys. Rev. B **78**, 134515 (2008).

[48] M. R. Ramadhan, I. Ramli, D. P. Sari, B. Kurniawan, A. Manaf, M. I. Mohamed-Ibrahim, S. Sulaiman, and I. Watanabe, Spin alignment studies on the muon-site determination in La_2CuO_4, Key Eng. Mater. **860**, 154 (2020).

[49] A. Andrade, T. Krikun, K. Schalm, and J. Zaanen, Doping the holographic Mott insulator, Nat. Phys. **14**, 1049 (2018).

[50] Y. Tokura, S. Koshihara, T. Arima, H. Takagi, S. Ishibashi, T. Ido, and S. Uchida, Cu-O network dependence of optical charge-transfer gaps and spin-pair excitations in single-CuO_2-layer compounds, Phys. Rev. B **41**, 11657 (1990).

[51] S. Uchida, T. Ido, H. Takagi, T. Arima, Y. Tokura, and S. Tajima, Optical spectra of $La_{2-x}Sr_xCuO_4$: Effect of carrier doping on the electronic structure of the CuO_2 plane, Phys. Rev. B **43**, 7942 (1991).

[52] S. Ono, S. Komiya, and Y. Ando, Strong charge fluctuations manifested in the high-temperature Hall coefficient of high-T_c cuprates, Phys. Rev. B **75**, 024515 (2007).